VI CHAPTER : THE ELECTRONIC STRUCTURE OF YH_X, LaH_X AND ELECTRON CORRELATION EFFECTS

VI.1 THE METAL-INSULATOR TRANSITION

One reason for the constant interest in the physics of rare-earth-metal-hydrides (REH_x), YH_x and LaH_x is the occurrence of a metal-insulator transition in these hydrides. The first unambiguous observation of a metal-insulator transition was done in 1969 by Libowitz et al.[1,2] on CeH_x for x around 2.8. This transition was somewhat peculiar since the sample was metallic at low temperature and insulating at high temperature. In a semiconducting material one observes the inverse tendency: the electrical resisitivity decreases when the temperature increases. A nice set of experimental data is shown in Fig. VI.1 for the case of LaH_x. For example, for x=2.90 the electrical resistivity exhibits "metallic" behaviour (positive $d\rho/dT$) from 125 K up to 240 K. Above this temperature the electrical resistivity increases rapidly by two orders of magnitude. At even higher temperature semiconducting behaviour i.e. $d\ln\rho/d(1/T)>0$ and constant) is observed. The corresponding energy gap is 480 meV. As a whole the resistivity changes from 19 $\mu\Omega$cm to 5×10^5 $\mu\Omega$cm between x=2 and 2.93. However, one should point out here that the electrical resistivity was measured by Shinar et al[3] using a contactless method on powder samples and that there may be some systematic error in the absolute values (but not in the trends). The presence of a tetragonal-to-cubic transition near or at the same temperature as the anomaly in resistivity suggests that the metal-insulator transition is first order.

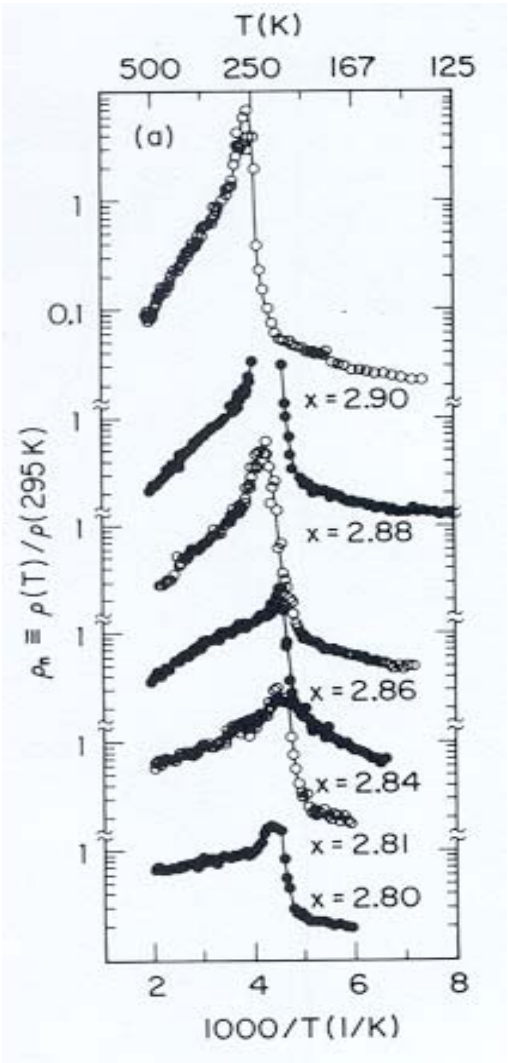

Fig. 30. Normalized resistivit
$\rho(T)/\rho(295\,K)$ of various La
mens as a function of reciproc
ature, showing the metal–sem

Fig. VI.1: Normalised electrical resistivity of a series of LaH_x samples as a function of reciprocal temperature. The sample with x=2.90 exhibits metallic behaviour at low temperature and semiconducting behaviour above 250 K. For the sample with x=2.80 X-ray diffraction measurements revealed a first order transition from a low temperature tetragonal phase to a high temperature cubic phase.

It is only very recently that a very detailed mapping of the temperature and concentration dependence of a REH_x-like hydride has been carried out. Hoekstra et al.[4] measured the electrical resistivity of YH_x from room temperature down to 300 mK for a whole series of hydrogen concentration and obtained the systematic behaviour shown in Fig.VI.2. According to scaling

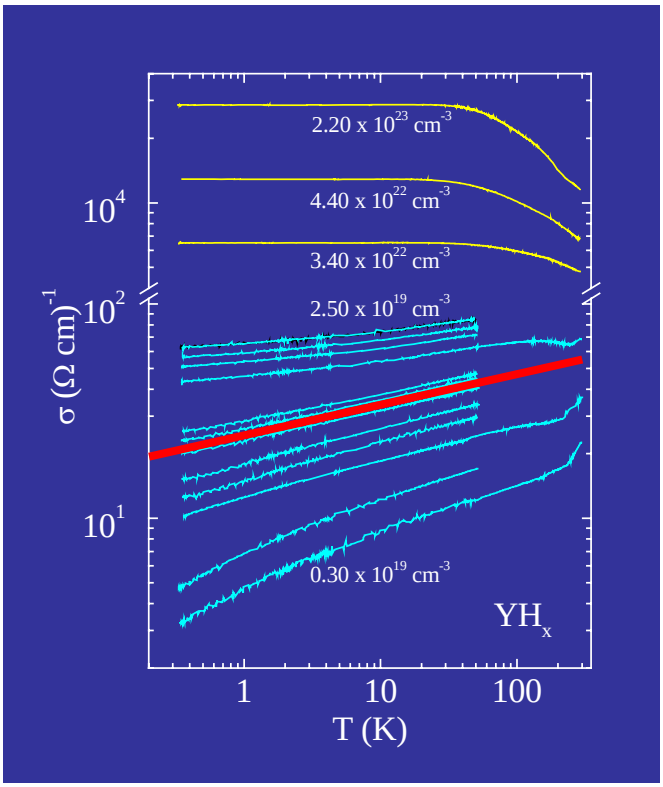

Fig.VI.2: Double-logarithmic representation of the temperature dependence of the electrical conductivity of a series of YH_x films. The curves re labeled with the measured charge carrier concentrations determined from Hall effect. The yellow curves correspond to YH_x metallic samples with $x<2.1$. The blue curves correspond to samples with $2.8 < x < 2.95$. The charge carrier concentration at the MI-transition (red line) is 1.35×10^{19} cm^{-3}.

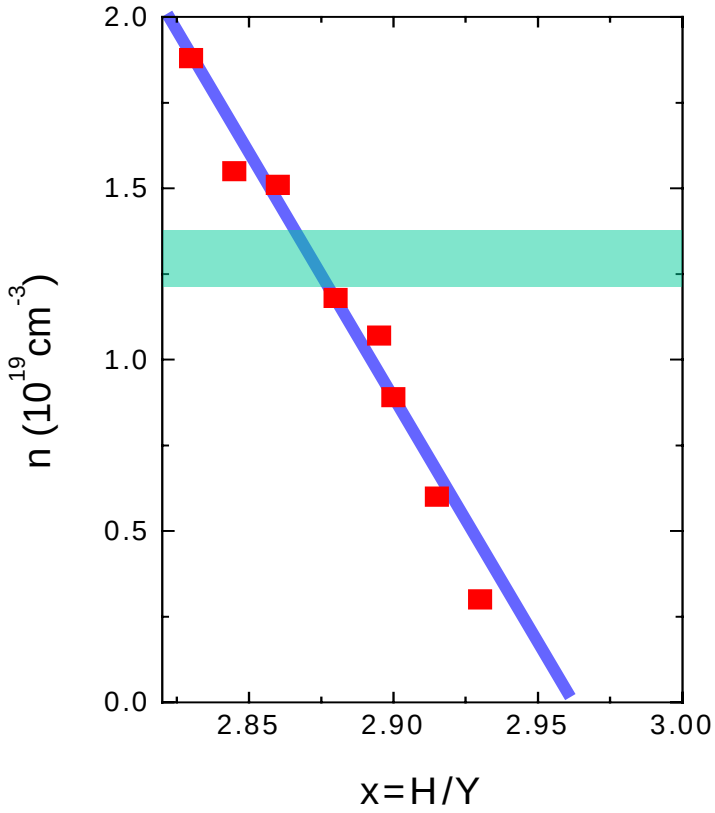

Fig. VI.3: Hydrogen concentration dependence of the charge carrier concentration of YH_x films as determined by Hoekstra et al. by means of Hall effect measurements. The accuracy of the hydrogen concentration is not better than a few percent. It is therefore possible that the fitted blue line should intercept the x-axis at 3. The green shaded region indicates the concentration range at which the metal-insulator transition takes place.

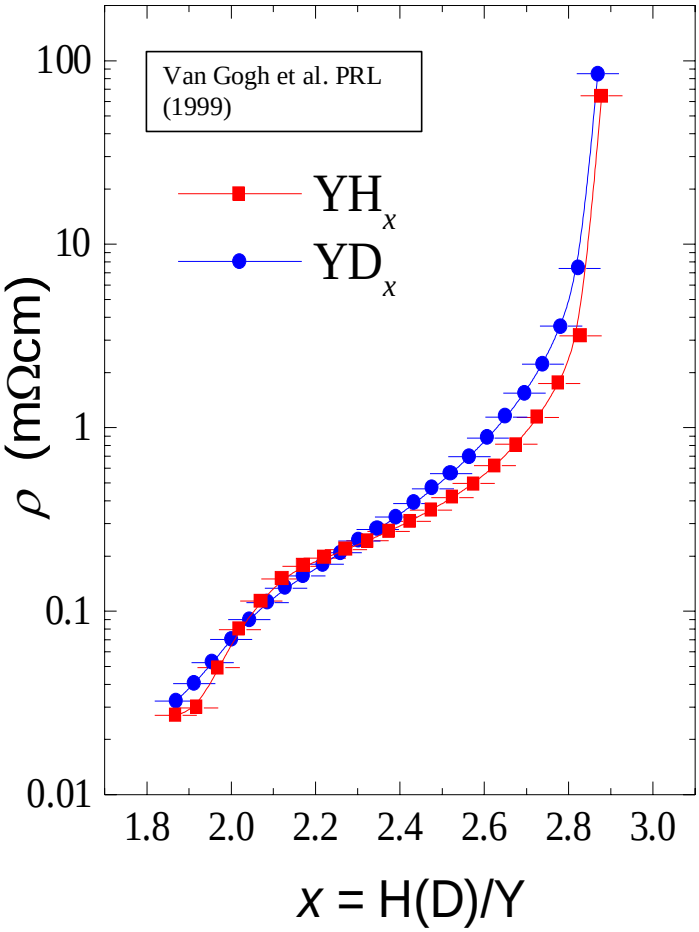

Fig.VI.4: Hydrogen (deuterium) concentration dependence of the room temperature electrical resistivity of a YH_x (YD_x) film. There is no isotope effect. The resistivity diverges for x~2.85

theories the metal-insulator transition occurs when the electrical conductivity exhibits power-law behaviour as a function of temperature. This corresponds to the red straight line in Fig.VI.2. From Fig. VI.3, we see that the corresponding hydrogen concentration is about 2.86. This is consistent with the room temperature measurements of Van Gogh et al that show a diverging behaviour of the electrical resistivity near the same concentration. It is important to note that the metal-insulator transition occurs at a **finite** concentration of charge carriers.

VI.2 SWITCHABLE MIRRORS

We give here a brief review of the switchable metal-hydride films discovered at the Vrije Universiteit in 1996. The purpose is to give some background information about the basic properties of YH_x and other metal-hydride films before discussing their electronic properties in the following sections and chapter VII (for the case of the complex metal-hydrides).
The content of this section is essentially the same as that of a review paper published by Griessen in Europhysics News[5]. An extended review article will be published by Wiley in 2005[6]

VI.2.1 THE DISCOVERY

In 1990, in the middle of the euphoric times of high-temperature superconductivity, researchers at the Vrije Universiteit in Amsterdam decided to search for other superconductors with a potentially high T_c but not based on copper and oxygen. Since there were predictions that solid, metallic atomic hydrogen might become superconducting at temperatures as high as 200-250 K, they looked into the possibility to create new superconductors based on hydrogen. However, instead of trying to metallize pure hydrogen under very high pressures, they chose another route. They first incorporated hydrogen into a metal to break the molecular bond of H_2 and started to compress the sample under high pressures (not higher than 0.5 GPa) to increase its metallic character, thus favoring superconductivity.

As starting material they chose yttrium, which is able to absorb 300% hydrogen up to the composition YH_3. They evaporated a 500 nm thick yttrium film on one of the diamonds of a high pressure diamond-anvil-cell. Quite unexpectedly, upon hydrogen uptake under several thousands of atmospheres, around 240 K, the yttrium film changed from a shiny metallic into a transparent yellowish sample[7]. Although metal-insulator transitions had already been described in earlier work on rare-earth hydrides[8], no report whatsoever existed about such drastic changes in their visible optical properties, most probably because nobody really looked at hydrides during hydrogen uptake. The great fortune of Hans Huiberts, the PhD student carrying out this work, was that the diamond-anvil-cell allowed him to optically monitor the hydrogen absorption *in situ*!

Very much intrigued by these spectacular changes, the Amsterdam team tried to induce the same transition at room temperature and low hydrogen gas pressure (typically 1 bar). It worked admirably, provided the yttrium film was protected by a thin layer (5-20 nm) of palladium. With this protective layer they could take samples out of the ultra-high vacuum deposition system without danger of oxidation (a severe problem with highly reactive materials such as yttrium and rare-earths) and carry out a whole series of *ex situ* experiments (temperature dependence of the resistivity, magnetoresistance, Hall effect, photoconductivity, pressure dependence of the semiconducting gap, optical transmission and reflection, etc.) which are usually impossible on the corresponding *bulk* materials as hydrogenation reduces their trihydrides into powder.

VI.2.2 OPTICAL SWITCHING

The simplest way to get an impression of what switchable mirrors really are is to follow the changes which occur in an yttrium film during loading with hydrogen at room temperature. Figure 1 exhibits the evolution of the electrical resistivity and optical transmission for red light (with $\hbar\omega$ = 1.96 eV) as a function of the time elapsed since the film has been brought into contact with hydrogen gas at 10^5 Pa. As the hydrogen uptake occurs approximately linearly, the time axis is essentially also a hydrogen concentration axis. Spectacular changes occur in both the electrical and optical properties. After a weak rise due to impurity scattering the electrical resistivity ρ decreases steadily until it reaches a minimum in the dihydride phase. YH_2 has at this point an electrical resistivity which is about 5 times *lower* than that of pure Y. At higher concentrations ρ increases by several orders of magnitude and is only limited by the conductivity of the 20 nm Pd caplayer. The optical transmittance remains low until in the dihydride phase a weak maximum occurs at approximately the same time as the minimum in ρ is reached. As demonstrated by Den Broeder *et al.*[9] this weak red transparency is most valuable for the

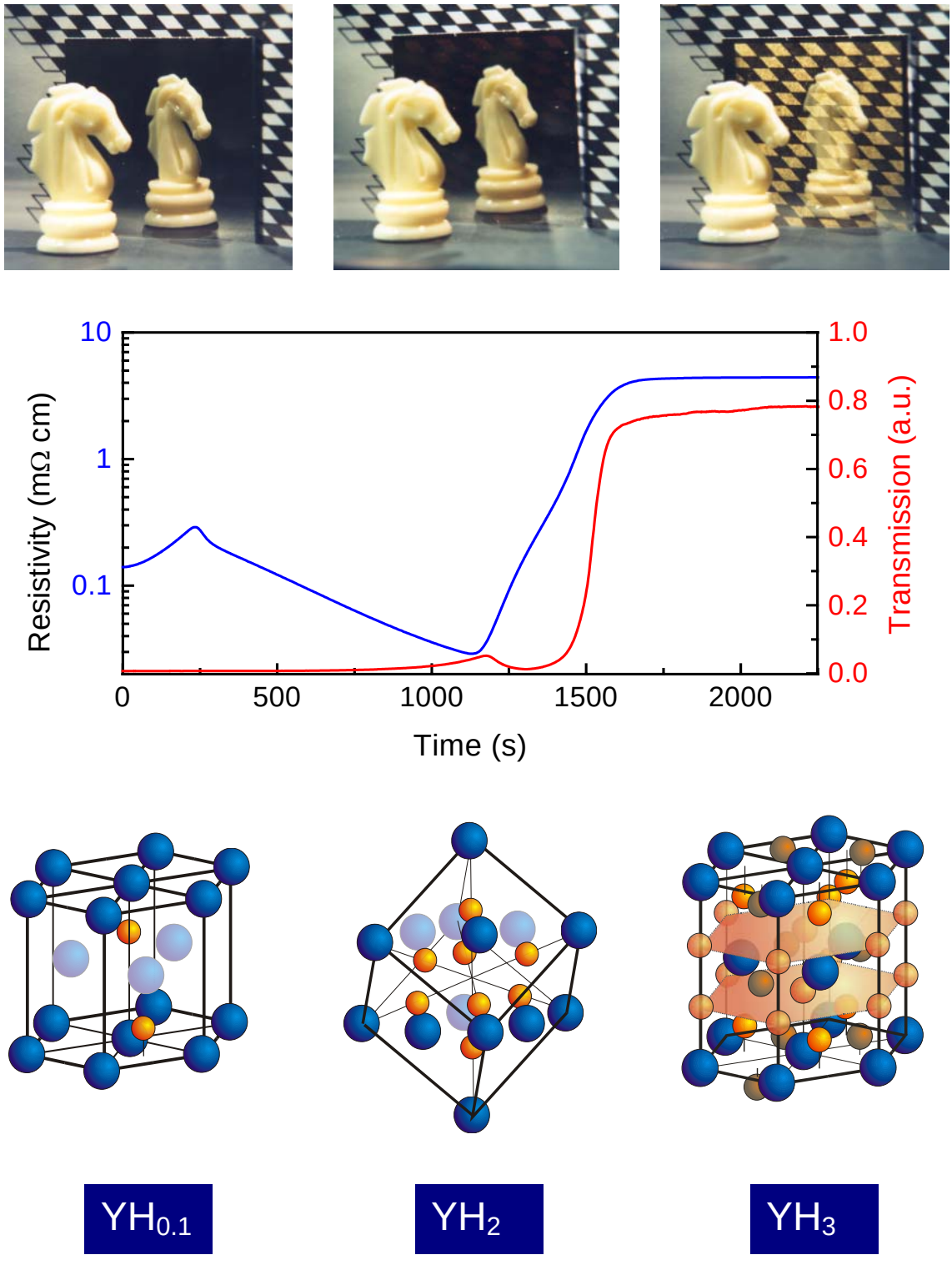

Fig. VI.5: Variation of the electrical resistivity and optical transmittance $\hbar\omega$ =1.96 eV) of a 300 nm thick yttrium film protected by a 20 nm thick Pd caplayer brought in contact with H_2 gas at 10^5 Pa pressure at room temperature. The hydrogen concentration is approximately proportional to the elapsed time t, except after 1600 s where both electrical resistivity and optical transmittance have reached saturation. This experiment is deliberately carried out slowly, but optical switching can in fact be much faster (see Fig. 4). The photographs illustrate the reflectance and transmittance of the film as deposited, in the dihydride and in the trihydride phase. The structures of the various phases are schematically depicted in the lower panel.

visualization of hydrogen diffusion as it makes it possible to locate exactly the YH_2 phase in a diffusion experiment. The film transmittance suddenly rises and stays high as the H concentration is increased from 2 to 3. These changes are easily observed as a switch from high to low reflectivity and significant transmittance in the last two photographs of Fig. VI.5. The transition back from the transparent trihydride to the shiny dihydride is reversibly induced by decreasing the surrounding hydrogen gas pressure. Gas loading is easily carried out; for a direct measurement of the hydrogen concentration it is necessary to use instead electrolytic charging. The time- integrated electrical current flowing in an oxygen-free electrolytic cell during hydrogen charging is a direct measure of the number of H injected into the switchable mirror. Measurements of optical transmittance and reflectance and other parameters as a function of H concentration are then possible. Whereas the drop in transmittance above $\hbar\omega$ = 2.8 eV in YH_3 in Fig. VI.6 is due to the onset of optical absorption, the oscillations in reflectance are due to interference within the sample.

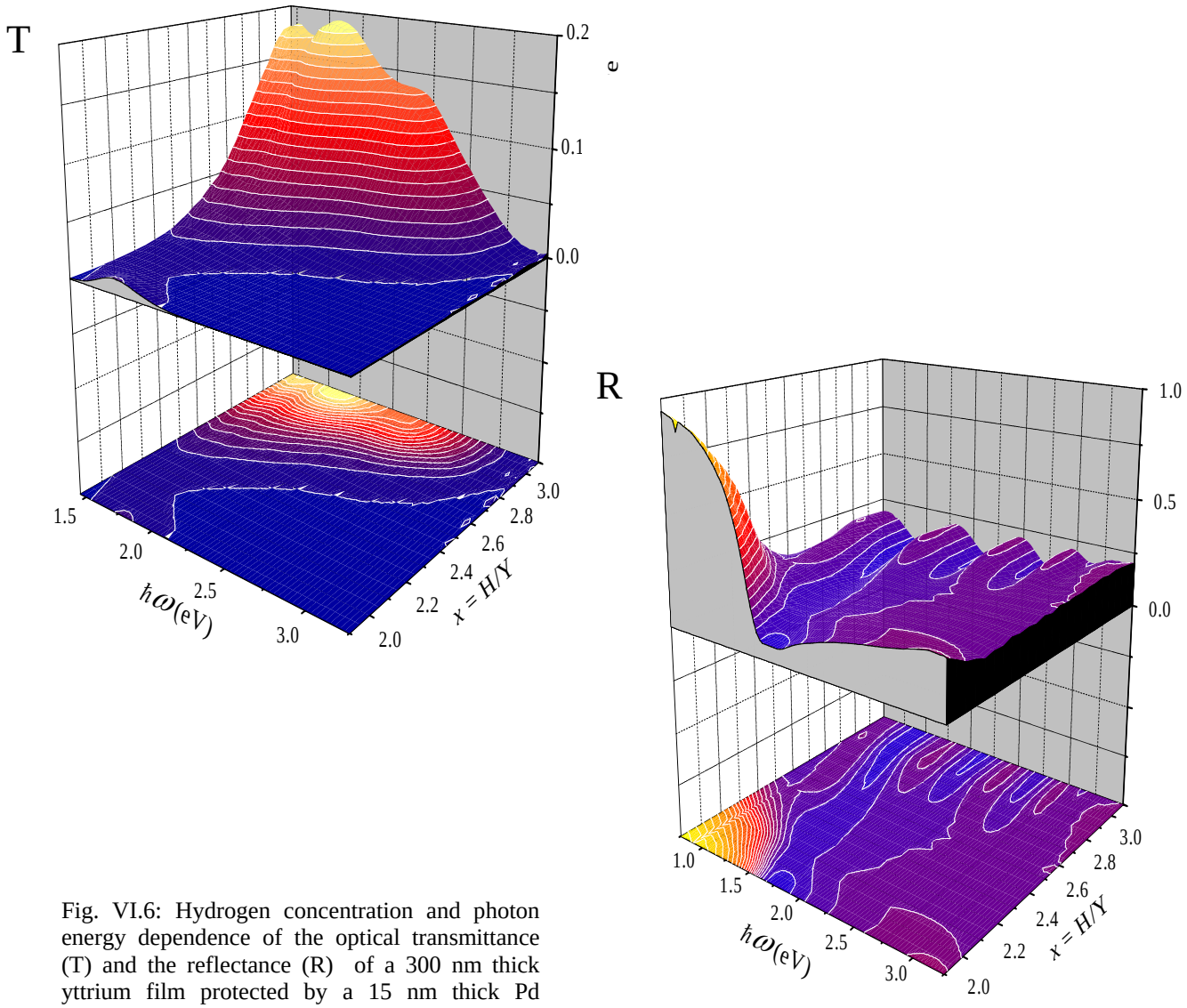

Fig. VI.6: Hydrogen concentration and photon energy dependence of the optical transmittance (T) and the reflectance (R) of a 300 nm thick yttrium film protected by a 15 nm thick Pd caplayer.

VI.2.3 METAL-INSULATOR TRANSITION

The increase in ρ with increasing H concentration in Fig. VI.5 (see also Fig.VI.2, Fig. VI.3, and Fig.VI.4) and the decrease of the reflectance in Fig. VI.6 are clear indications of the occurrence of a metal-insulator (MI) transition. At first sight this MI-transition seems to have a rather trivial origin. As seen in Fig. VI.5, YH_2 has a cubic structure while YH_3 is hexagonal. Many such MI-transitions in nature are first order (for example diamond to graphite, white to grey tin, vanadium oxides). However, it was shown that YH_x is already in the hexagonal phase when the MI-transition occurs around x=2.86: the metal-insulator transition is thus not connected to a structural phase transition. YH_x is, therefore, one of the very few examples of a system with a *continuous* MI-transition; this alone makes it a fascinating material. In addition, the ease at which the H concentration can be modified is a tremendous advantage for experimental investigations. Instead of having to painstakingly prepare a whole series of samples with various degrees of doping (for example boron doped silicon, or Se substituted NiS_2) one can simply actuate a switchable mirror by controlling the surrounding hydrogen gas pressure or the voltage in an electrolytic cell.

The MI-transition is also *robust* in the sense that it occurs in all hydrides of the trivalent rare-earths. They all switch optically when the H concentration is increased from 2 to 3 although the crystal structure of the trihydrides can be *hexagonal* as for YH_3, *cubic* as for LaH_3 or more complicated as for SmH_3. A MI-transition also occurs in *cubic* YH_3 and in disordered alloys of yttrium and lanthanum, whose trihydrides are either cubic or hexagonal, depending on the composition.[10] In the trihydride state they are all transparent albeit with characteristic colors: for example, YH_3 is yellowish, LaH_3 red, while some alloys are colorless.

VI.2.4 THEORETICAL MODELS

Although the occurrence of a MI-transition in YH_x could have been expected on the basis of earlier work on bulk rare-earth hydrides [1, 2] the transparency of $YH_{3-\delta}$ discovered by Huiberts et al. came as a great surprise, since the state-of-the-art self-consistent band structure calculations in the early nineties predicted YH_3 to be a semi-metal (see Section VI.4) with, in fact, a considerable band *overlap* (1.5 eV). The occurrence of large optical gaps in YH_3 and LaH_3, as well as the observed increase in resistivity with decreasing temperature, being incompatible with a metallic character, stimulated theorists to reconsider the YH_x and LaH_x systems in detail. Somewhat as for the high-T_c superconductors two lines of thought developed:

i) Band structure models: Originally it was proposed that the semiconducting ground state of YH_3 was due to a so-called Peierls distortion (see Section VI.5) of the crystal lattice. The total energy of YH_3 was indeed found to be extremely sensitive to the exact position of the H atoms, especially those close to the Y planes. So far, however, no experimental evidence has been found for the existence of a low symmetry crystal structure of YH_3. Very recently van Gelderen *et al.*[11] demonstrated that improved band structure calculations based on the so-called GW approximation led to a fundamental direct but dipole forbidden energy gap of 1 eV and an indirect optical gap of almost 3 eV without having to invoke any lattice distortion. The agreement of these calculations with the optical data is remarkable since they do not involve any fit parameters. A similar approach predicted that also *cubic* YH_3 should be a semiconductor.

ii) Strong electron correlation models: Other theorists[12] expected strong correlation effects to be especially large in YH_x and similar rare-earth-hydrides as a direct consequence of the large on-

site repulsion between two electrons near the same proton. This repulsion is reflected in the radius of the negative H^--ion (see Section VI.6.1) that is about 3 times larger than for a neutral H atom and its ionization potential, which is only 0.7 eV compared to 13.6 eV for neutral H. Electron correlation leads to a drastic narrowing of the H-derived band and therefore to a sizeable gap between this low-lying band and the La-derived 5d-bands in LaH_x or the Y-derived 4d-bands in YHx. The swelling of neutral H when it transforms to an H^--ion led to the new concept of a breathing Hubbard Hamiltonian (see Section VI.6.4).

The GW calculations provide no direct insight into the mechanism of the metal-insulator transition. The strong electron correlation picture, however, leads to the following scenario first proposed by Sawatzky and co- workers. For simplicity, we consider the case of LaHx. Although metallic La is hexagonal, LaH_2 is cubic with all tetrahedral sites occupied by H atoms (CaF_2 structure). These H atoms are so strongly bound that they are not involved in the MI-transition that occurs around $LaH_{2.8}$. The nice thing about LaH_x at room temperature, is that it remains cubic all the way up to LaH_3. Each H added to LaH_3 occupies octahedral sites with six La nearest neighbors. It attracts a conduction electron to form a singlet in a way similar to what happens with two holes in high-T_c superconducting cuprates. One electron is on an orbital localized around the proton (with a radius of $\simeq$ 0.5 Å) and the other is race-tracking on the neighboring La

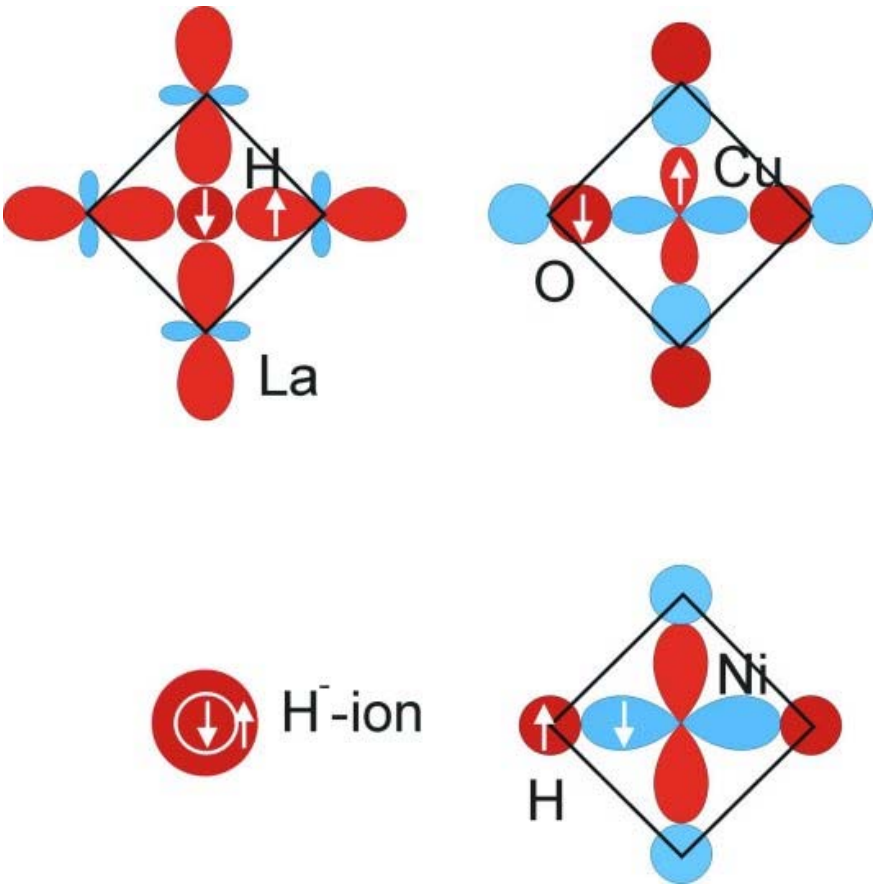

Fig. VI.7: Correlated singlet states depicted in a plane as antisymmetrized products of atomic-like orbitals. Lobes of opposite sign are shown in red and blue. In $LaH_{2+\delta}$ the singlet involves two electrons and resembles locally a huge H^--ion. In a cuprate such as La_2CuO_4 and the hydride Mg_2NiH_4 it involves two holes at the top of the metal-derived d-band.

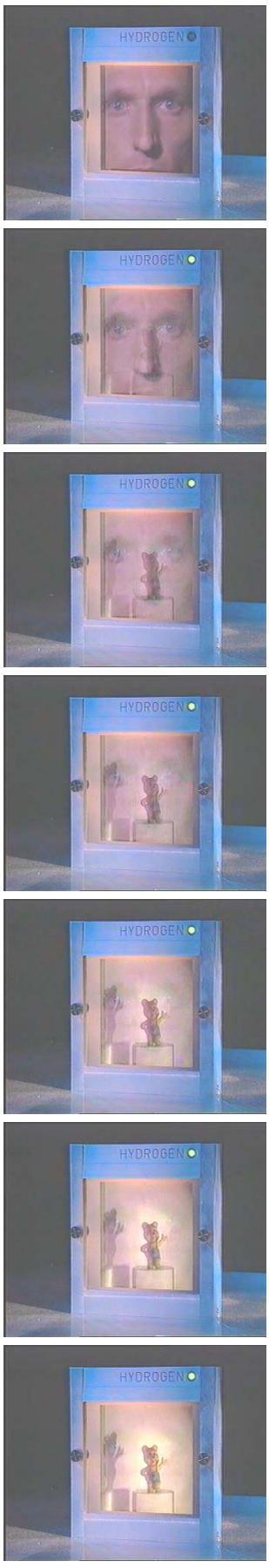

atoms (see Fig. VI.7). Roughly speaking this resembles a huge H^--ion with a diameter of the order of the host lattice spacing (≈ 6 Å). As every H ties up an electron from the conduction band, electrical conductivity becomes increasingly difficult and the system tends towards a so- called Kondo-insulator. In an alternative picture, one may start from insulating LaH_3 and create vacancies in the octahedral H sublattice. Ng et al.[13] argue that H^- vacancies are highly localized donors. This explains why 0.2 vacancies per La (a huge doping level compared to those usually involved in semiconductors) are required to create a band from overlapping donor wave functions and to drive the system metallic around $LaH_{2.8}$. The steady increase of charge carrier density with increasing vacancy density (i.e. decreasing x) is confirmed by Hall effect measurements (see Fig. VI.3).

The attractiveness of the strong-correlation picture is that it is local and therefore inherently robust. It is marginally affected by disorder or the overall crystal structure. It also provides a direct explanation for the effective negative charge of H observed in electromigration experiments and the puzzling result of van der Molen *et al.*[14] that, at high temperatures, when H diffuses rapidly, the flux of H atoms measured in $YH_{3-\delta}$ by means of electromigration is equal to the current of electrons. It looks as if during a diffusion jump of a proton, one of the electrons in the original singlet is momentarily lent to the conduction band to be recaptured somewhat later at a neighboring site to reform a singlet.

Fig. VI.8: Frames of a video taken during hydrogen absorption by a GdMg switchable mirror[15]. The indicator lights up when gaseous H_2 is introduced in the system. The mirror image of the experimenter fades out rapidly while the little toy bear behind the mirror appears. The time between the first and last frame is 280 ms. The characteristic switching time is less than 40 ms. (Courtesy P. Duine, Philips Research Labs., Eindhoven).

VI.2.5 SECOND GENERATION SWITCHABLE MIRRORS

A major step towards applications was set in 1997 when Van der Sluis *et al.*[16] reported that $Gd_{1-y}Mg_yH_x$ alloys with $y > 0.4$ could be made transparent and colorless in contrast to the yellowish YH_3 (see Fig. VI.5). Moreover, the contrast between reflecting and transparent states is enhanced due to the absence of the weak transparency maximum, which is characteristic for YH_2, LaH_2 or REH_2 in their metallic state. In addition $Gd_{1-y}Mg_yH_x$ mirrors switched fast: as shown in Fig. VI.8, the transition from the metallic state to the transparent insulating state occurs in less than 40 ms. The optical gap of $Gd_{0.5}Mg_{0.5}H_{2.5}$ being 3.4 eV, this switchable mirror is color neutral. This color neutrality has also been observed in Y-Mg and La-Mg alloys and is probably a general property of Mg-rare earth alloys. The possibility to fine-tune the optical gap is most important for applications of switchable mirrors.
From a fundamental point of view these Mg-containing alloys confronted the Amsterdam researchers with a new switching process. During the first hydrogen absorption $Y_{0.5}Mg_{0.5}H_x$ disproportionates first into YH_2 and Mg and subsequently, after formation of MgH_2, into a transparent composite of MgH_2 and YH_3. This composite switches back to a metallic composite of YH_2 and Mg . In this transformation Mg acts as a sort of *microscopic shutter* since it switches reversibly from an excellent metal to a large gap (about 6 eV) insulator. This suggested that multilayers of Y (or any rare-earth) and Mg would also act as color neutral switchable mirror which was indeed confirmed experimentally. This is at first sight not extremely surprising since MgH_2 has a much larger optical gap (approx. 6 eV) than YH_3. What is not trivial at all, however, is that the electrical resistivity of $Y_{0.75}Mg_{0.25}H_{2.75}$ is *four* orders of magnitude larger than that of $YH_{3-\delta}$! This cannot be understood in terms of a simple disproportionation and indicates that electronic effects are occurring at the Y-Mg interface.

VI.2.6 THIRD GENERATION SWITCHABLE MIRRORS

Recently, Richardson *et al.*[17] (Lawrence Berkeley Labs.) reported that a thin film of a Mg-Ni alloy also exhibited optical switching. This is a major extension of the class of switchable mirrors since it avoids Y, La or rare-earth metals. It is also of fundamental importance since the transparent phase is probably Mg_2NiH_4, a compound in which H and Ni orbitals hybridize strongly to form covalently bonded $(NiH_4)^{4-}$-complexes that are bound ionically to Mg^{2+}-ions (see Chapter VII). The gap is essentially determined by the most antibonding Ni-H state at the top of the d-band of nickel (see Fig. VI.7), a situation similar to that in cuprates (for example in La_2CuO_4). Since Mg_2CoH_5 and Mg_2FeH_6 can also be formed, it is probable that new switchable mirror materials based on such compounds will be discovered. This opens a completely new field of investigation of materials with remarkable optical properties in the visible part of the spectrum.

VI.2.7 EPITAXIAL SWITCHABLE MIRRORS

So far we have described electrical and optical properties of *polycrystalline* switchable mirrors. We found that it was also possible to synthesize YH_x *epitaxial* films on a transparent and electrically insulating substrate with evaporation at high temperature on a (111)-CaF_2 substrate. The crystallinity of these films deduced from X-ray diffraction is excellent and remains so even after repeated hydrogen loading and unloading. This is in itself remarkable since there is a 15% volume expansion between Y and YH_3! The process through which an epitaxial film can accommodate such high strains without deterioration of its crystallinity was recently

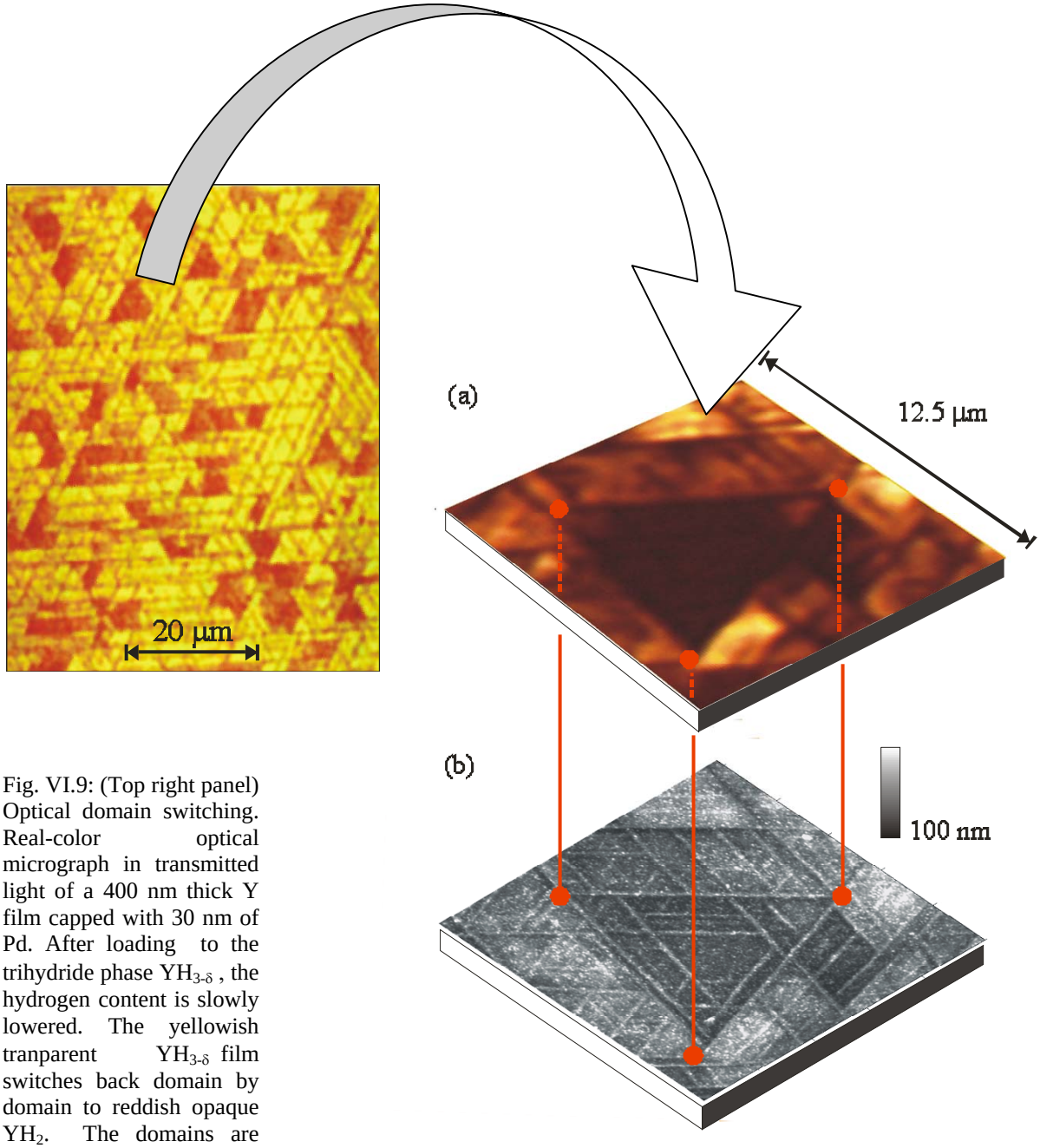

Fig. VI.9: (Top right panel) Optical domain switching. Real-color optical micrograph in transmitted light of a 400 nm thick Y film capped with 30 nm of Pd. After loading to the trihydride phase $YH_{3-\delta}$, the hydrogen content is slowly lowered. The yellowish tranparent $YH_{3-\delta}$ film switches back domain by domain to reddish opaque YH_2. The domains are bounded by a triangular network of reddish opaque lines.

(Right panels) One-to-one correlation between optical and structural texture. **a)** Optical micrograph in transmitted light of a dihydride/trihydride mixed phase region of a 150 nm thick Y/CaF_2 film capped with 20 nm of Pd. The image is 12.5x12.5 μm^2. The large triangle is almost entirely in the electrically conducting and opaque dihydride phase (YH_2). The bright yellow regions are in the transparent trihydride phase (YH_3). **b)** AFM micrograph of the same area as in Fig 2a. A triangular network of ridges bounds micron-sized flat domains of various heights (dark is low, white is high) . The surface topography closely matches the optical pattern in Fig. 2a, indicating that domains are in different stages of switching from YH_2 (opaque, contracted domains) to YH_3 (transparent, expanded domains).

identified by Kerssemakers *et al.*[18] Using *in situ* Atomic Force Microscopy, combined with electrical resistivity and local optical transmission measurements, they discovered that micron-sized triangular domains switch one-by-one, homogeneously and essentially independently, during hydrogen absorption. These optically resolvable domains are defined by an extended self-organized ridge network, created during the initial hydrogen loading. The ridges block lateral hydrogen diffusion and act as a microscopic lubricant for the sequentially expanding and contracting domains. This block-wise switching results in a 'Manhattan skyline' in which optical and structural texture are intimately correlated. Their tunability is of technological relevance since it opens the way to a pixel- by-pixel switchable pattern with a minimal amount of inactive surface area. The domain switching of epitaxial films is *locally* very different from the behavior of polycrystalline films, which are optically homogeneous on a micrometer length scale. However, on a macroscopic scale, both polycrystalline and epitaxial switchable mirrors exhibit the same properties.

VI.2.8 OUTLOOK

The great richness of new phenomena in the electrical, optical and mechanical properties of switchable mirror materials, the possibility to fine-tune their properties by alloying and the ease to change continuously their hydrogen content makes them especially attractive for fundamental condensed matter physics. Detailed studies of continuous metal-insulator transitions, fast diffusion and electromigration are drastically simplified since i) the concentration of the dopant (hydrogen) can be modified at will by simply changing the surrounding gas pressure or the voltage in an electrolytic cell, and ii) hydrogen migration can easily be monitored visually. Replacement of hydrogen by deuterium also offers unique opportunities to investigate isotope effects in many physical properties.

They offer also interesting possibilities for technological applications, such as smart windows to regulate the light and heat transfer in buildings, antireflection coatings for TV screens and monitors, variable reflectance rear-view mirrors in cars, variable transmittance glasses and smart light bulbs with adaptive optics. Epitaxial switchable mirrors may offer additional possibilities through their self-organized, pixel-by-pixel switchable domain pattern. Recently, two groups at Lawrence Berkeley and at Philips Research Labs have demonstrated the feasibility of all-solid-state devices based on metal-hydride switchable mirrors. In such devices, the mirror layer is separated from a conducting transparent layer of indium-tin oxide by a solid electrolyte (e.g. ZrO_2). Applying a voltage one can control the hydrogen concentration in the switchable mirror and induce reversible switching. Although many materials problems still remain to be solved, such all-solid-state devices are an important step towards large-scale application of switchable mirrors.

Recently it was discovered that certain switchable mirrors do not simply switch from shiny metallic to transparent during hydrogen loading. They also exhibit a highly absorbing black state at intermediate h concentration. It took a long time to understand the microscopic mechanism responsible for this black state but by now it is clear that it arises because of a peculiar self-organised layering of the film during absorption of hydrogen. This black state is presently exploited in switchable solar collectors and hydrogen optic fibre sensors.

After this brief introduction to switchable mirrors we return now to the original topic of this chapter, the electronic structure of YH_x and similar REH_x systems.

VI.3 ELECTRONIC STRUCTURE OF Y- AND LA-HYDRIDES

Already in 1971 Switendick[19] calculated the electronic band structure Y, YH_1, YH_2 , and YH_3 assuming a cubic crystal structure for all compounds. This does not correspond to the real structures (except for YH_2 that does have the cubic CaF_2 structure) but is very useful for illustrating the effect of hydrogen on the band structure of the host metal. As discussed in Chapter V the monohydride is characterized by the appearance of **one** low-lying band and the dihydrides by **two** low-lying bands. Interesting is the opening of a 2 eV gap in the trihydride.

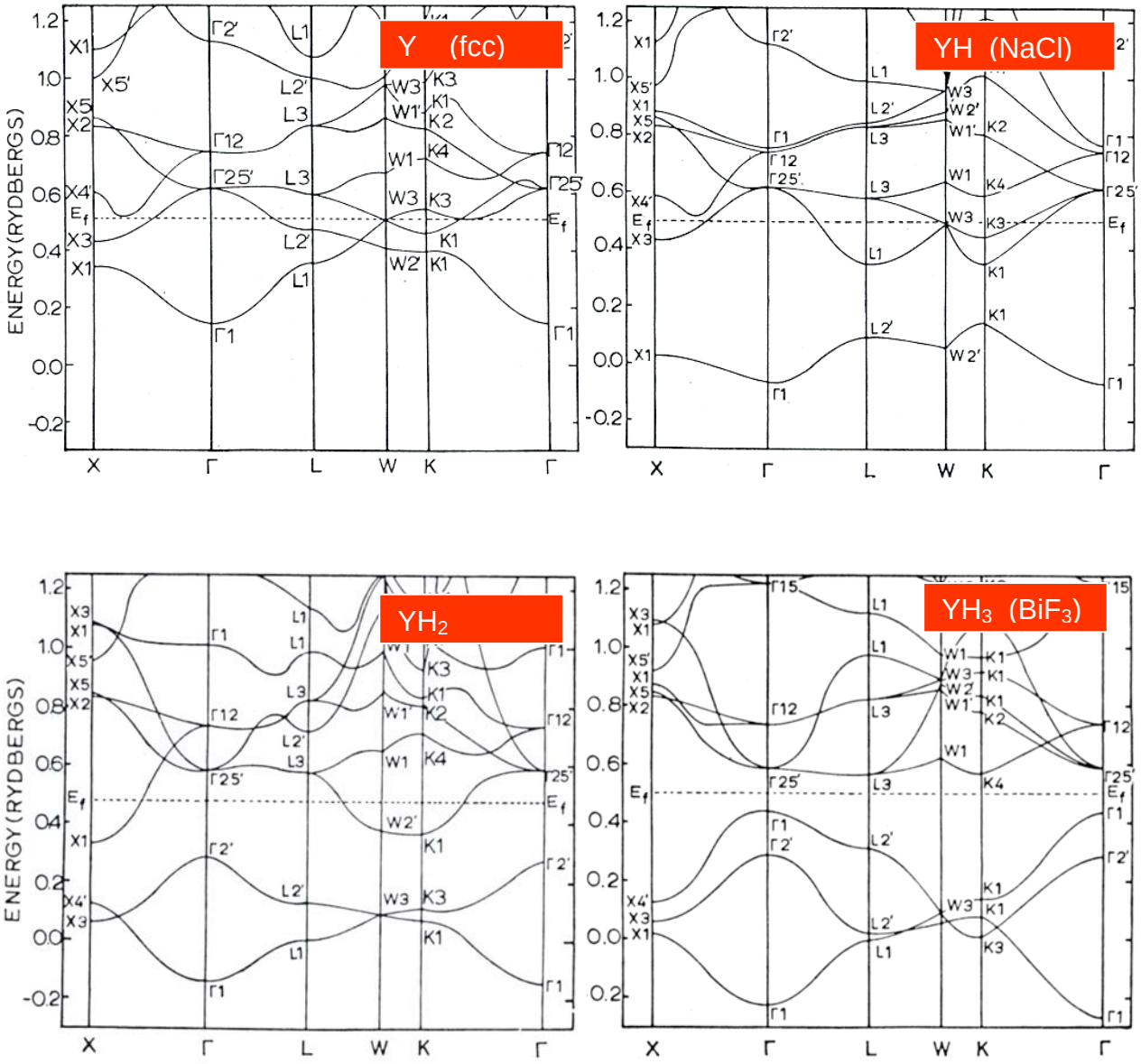

Fig. VI.10: Electronic band structures of hypothetical cubic Y, YH_1, YH_2 , and YH_3 calculated by Switendick with non-self consistent potentials. The trihydride is predicted to be an insulator with a gap of the order of 2 eV (Note that 1 Rydberg=13.6 eV). The Brillouin zone is the same for all four structures (see Fig.V.1).

The existence of three low-lying bands in the trihydride can be understood in the same way as the apparition of two low-lying bands in the dihydride.

VI.4 ELECTRONIC STRUCTURE OF TRIHYDRIDES

The formation of three low-lying energy bands can easily be understood from the following linear model. The metal atoms are on a linear chain arrangement and have now three hydrogen neighbours each. One construct first molecular orbitals for each MH_3 building block (see Fig. VI.11 and incorporate them later into a tight-binding calculation. The elementary building block consists of two tetrahedral and one octahedral hydrogen. The distance between two neighbouring tetrahedral hydrogen is a/2 while the distance between a octahedral hydrogen and a tetrahedral hydrogen is $\sqrt{3}a/4$. The overlap integral between two tetrahedral hydrogen is thus smaller than between a tetrahedral and an octahedral hydrogen.

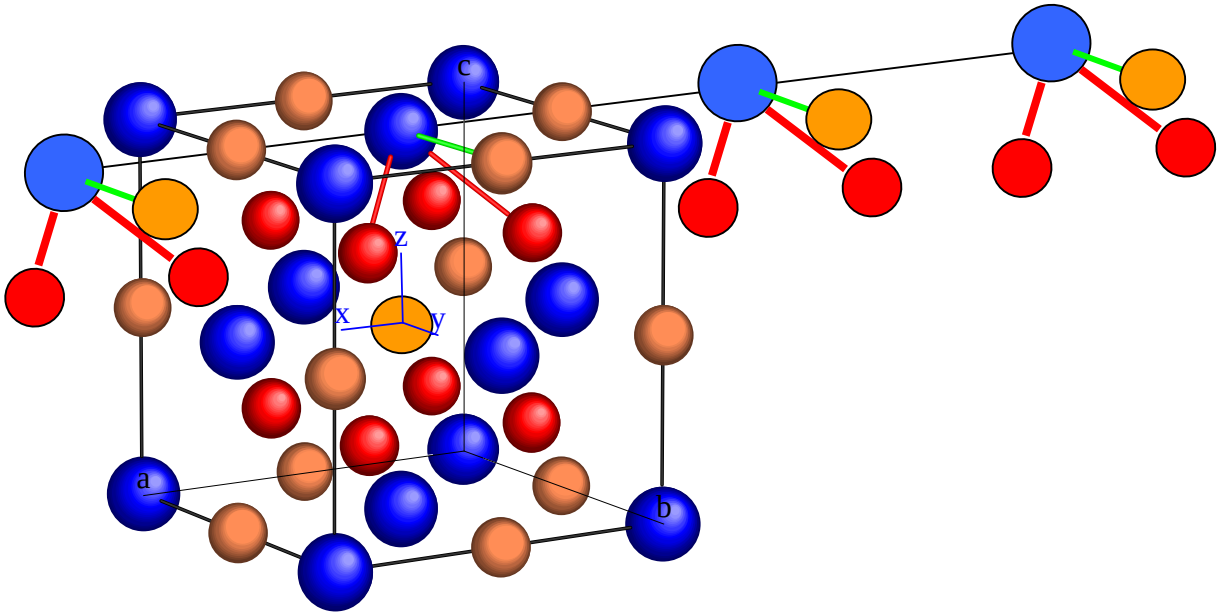

Fig. VI.11: The BiF_3 structure assumed for the electronic band structure calculations of YH_3. The metal atoms (blue) are on a FCC lattice. The hydrogen atoms at tetrahedral interstitial sites (red) form a simple cubic lattice of lattice constant a/2. These are the hydrogen atoms considered for the linear model of the di-hydrides in Chapter V. The hydrogen at octahedral sites (orange) form together with the metal atoms a NaCl structure. The elementary building block (we show several of them) consists of two tetrahedral and one octahedral hydrogen. The distance between two neighbouring tetrahedral hydrogen is a/2 while the distance between a octahedral hydrogen and a tetrahedral h is $\sqrt{3}a/4$.

In analogy with the dihydride problem considered in Chapter V we introduce the following notations for simplification

$$\overline{H}_i \equiv -\frac{\hbar^2}{2m}\Delta + V(\mathbf{R}_i - \mathbf{r}) \qquad \text{(i=M, L, R, O)} \qquad \text{(VI.1}$$

where M stands for metal, and L and R for the left and right hydrogen atoms on tetrahedral sites and O for the hydrogen atom at the octahedral position, respectively. The atomic wave functions are for hydrogen

$$|L\rangle \equiv \phi_G(\mathbf{L}-\mathbf{r}) \qquad |\,\mathrm{R}\rangle \equiv \phi_G(\mathbf{R}-\mathbf{r}) \qquad \text{(VI.2}$$

and for the metal (we assume in the following the it is a metal s-state)

$$|M\rangle \equiv \phi_M(\mathbf{R}_M - \mathbf{r}) \qquad \text{(VI.3}$$

and correspondingly for the potentials

$$V_L \equiv V(\mathbf{L}-\mathbf{r}) \qquad V_R \equiv V(\mathbf{R}-\mathbf{r}) \qquad \text{and } V_M \equiv V(\mathbf{R}_M - \mathbf{r}) \qquad \text{(VI.4}$$

We have

$$\overline{H}_L|L\rangle \equiv \left[-\frac{\hbar^2}{2m}\Delta + V_L(\mathbf{r})\right]|L\rangle = E_H|L\rangle \qquad \text{(VI.5}$$

for the hydrogen atom on the left. A similar expression applies for the proton on the right and for the proton at the octahedral site. E_H is the ground state energy of the hydrogen atom. For the metal, we analogously

$$\overline{H}_M|M\rangle \equiv \left[-\frac{\hbar^2}{2m}\Delta + V_M(\mathbf{r})\right]|M\rangle = E_M|M\rangle \qquad \text{(VI.6}$$

We seek a solution of the Schrödinger for one electron

$$\left[-\frac{\hbar^2}{2m}\Delta + V_M(\mathbf{r}) + V_L(\mathbf{r}) + V_R(\mathbf{r})\right]\Psi = E\Psi \qquad \text{(VI.7}$$

as a linear combination of the atomic states $|M\rangle, |R\rangle, |\mathrm{L}\rangle$ and $|\mathrm{O}\rangle$, i.e.

$$\Psi = a|M\rangle + b|L\rangle + \mathrm{c}\,|R\rangle + d|\mathrm{O}\rangle \qquad (\text{VI.8}$$

Following the usual three steps indicated in chapter II we find, neglecting three-center overlap integrals,

$$\begin{aligned} &a\left[E_M + \langle M|V_L|M\rangle + \langle M|V_R|M\rangle + \langle M|V_0|M\rangle\right] + \\ &+ b\langle L|\ V_L|\ M\rangle + c\langle R|\ V_R|\ M\rangle + d\langle O|\ V_0|\ M\rangle = E\,a \end{aligned} \qquad (\text{VI.9}$$

and

$$\begin{aligned} &a\langle M|\ V_M|\ L\rangle + b\left[E_H + \langle L|V_M|L\rangle + \langle L|V_R|L\rangle + \langle L|V_0|L\rangle\right] \\ &+ c\langle R|\ V_R|\ L\rangle + d\langle O|\ V_0|\ L\rangle = E\,b \end{aligned} \qquad (\text{VI.10}$$

and a similar expression for the hydrogen wave function on the right tetrahedral site and for the octahedral site. This leads to the following matrix

$$\begin{pmatrix} E_M - 3V & -t & -t & -t \\ -t & E_H - 3V & -t & -t_0 \\ -t & -t & E_H - 3V & -t_0 \\ -t & -t_0 & -t_0 & E_H - 3V \end{pmatrix} \begin{pmatrix} a \\ b \\ c \\ d \end{pmatrix} = E \begin{pmatrix} a \\ b \\ c \\ d \end{pmatrix} \qquad (\text{VI.11}$$

in which, for simplicity, we have set (we give only some examples)

$$\langle M|\ V_M|\ L\rangle = \langle R|\ V_R|\ L\rangle = \langle M|\ V_M|\ O\rangle = -t \qquad (\text{VI.12}$$

$$\langle L|V_M|L\rangle = \langle L|V_0|L\rangle = \langle R|V_M|R\rangle = \langle M|V_R|M\rangle = -V \qquad (\text{VI.13}$$

although in reality the M-H and M-M tunnelling matrix elements might be different from each other and similarly the Coulomb terms might differ from –V. These refinements are however irrelevant for the present qualitative discussion. On the other hand we have to take into account that the three hydrogen atoms are not equivalent. This is the reason why we have introduced the overlap integral

$$\langle O|\ V_R|\ R\rangle = \langle O|\ V_L|\ L\rangle = \langle O|\ V_O|\ L\rangle = -t_o \qquad (\text{VI.14}$$

There exists a non-trivial solution if the following secular determinant vanishes

$$\begin{vmatrix} E_M - 3V - E & -t & -t & -t \\ -t & E_H - 3V - E & -t & -t_0 \\ -t & -t & E_H - 3V - E & -t_0 \\ -t & -t_0 & -t_0 & E_H - 3V - E \end{vmatrix} = 0 \qquad \text{(VI.15}$$

There are four energy eigenvalues and eigenvectors. As an illustration we consider a numerical example with of E_H=-10 eV, E_M=-4 eV, V=0, t=2 (for the tetrahedral sites) eV and t_0=3 eV (overlap of the octahedral and tetrahedral hydrogen states). The energy eigenvalues are (with the corresponding eigenvectors given in parentheses),

E_1=-16.33 eV (0.27, 0.54, 0.54, 0.59) (VI.16

E_2=-8.0 eV (0, -0.707, 0.707, 0) (VI.17

E_3=-6.65 eV (0.05, 0.43, 0.43, -0.79) (VI.18

E_4=-3.02 Ev (0.96, -0.17, -0.17, -0.13) (VI.19

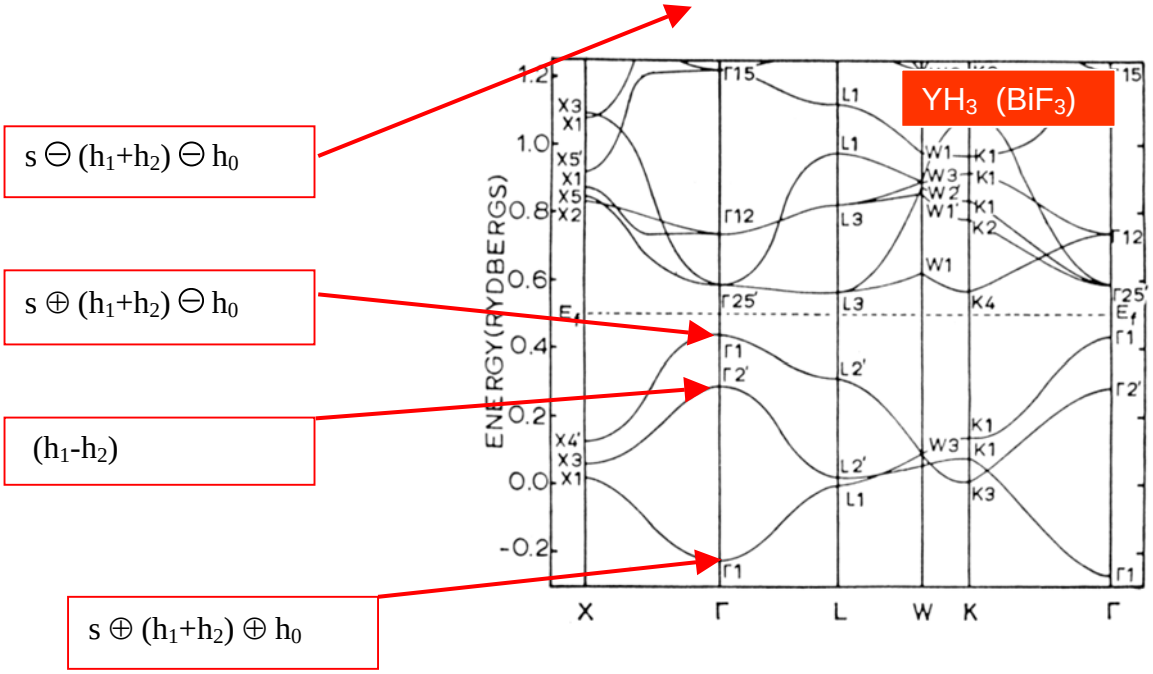

Fig. VI.12: Band structure of YH_3 calculated by Switendick together with the combinations of atomic wave functions contributing to hydride band states. The notation is obviously related to the eigenvectors given in Eqs.VI.15 to 17.

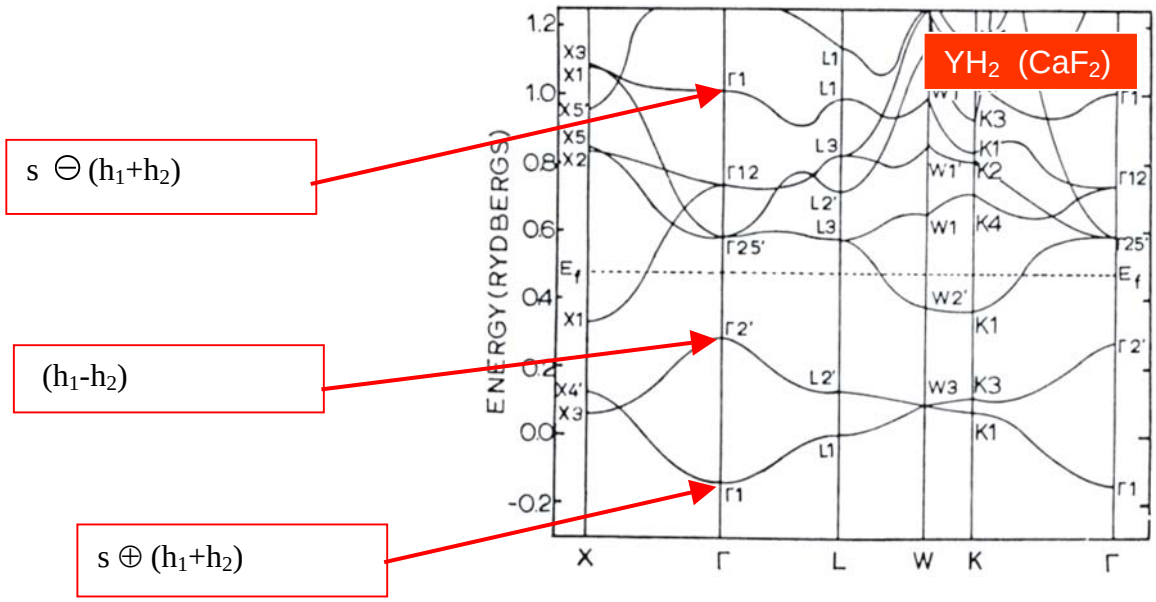

Fig. VI.13: Band structure of YH_2 calculated by Switendick together with the combinations of atomic wave functions contributing to hydride band states. The notation is obviously related to the eigenvectors given in Eqs.V.50 to 52.

Interestingly, the eigenvector corresponding to the energy E_2 is still independent of the chosen parameters and has

$$a = 0, \quad b = -\frac{1}{\sqrt{2}} \quad , \quad c = \frac{1}{\sqrt{2}} \quad \text{and} \quad d = 0 \qquad \text{(VI.20}$$

i.e. this state corresponds to the antibonding state of the H_2 molecule in absence of electro-electron interaction. It has zero admixture of the metal atomic wave function. The other three states involve linear combination of all four atomic states, but the coefficients b and c are always equal to each other in magnitude. This is the reason why Switendick labels these states as indicated in Fig. VI.12 and Fig. VI.13 (for the dihydride, please look at the calculation given in Chapter V for the linear chain of MH_2 building blocks).

At this point one might get the impression that the characteristic features of dihydrides and trihydrides are understood since the band structures of Switendick predict a metallic state for YH_2 and an insulating state for YH_3. In fact the discovery of the switchable mirrors and the band structure results of Dekker et al[20] and Wang and Chou[21] in the early nineties led to a surprising situation: state-of-the-art band structure calculations predicted that YH_3 should be a metal while the experiment showed that YH_3 was a semiconductor ! A nice example of a calculation that implies that a trihydride should be metallic is shown in Fig. VI.14.

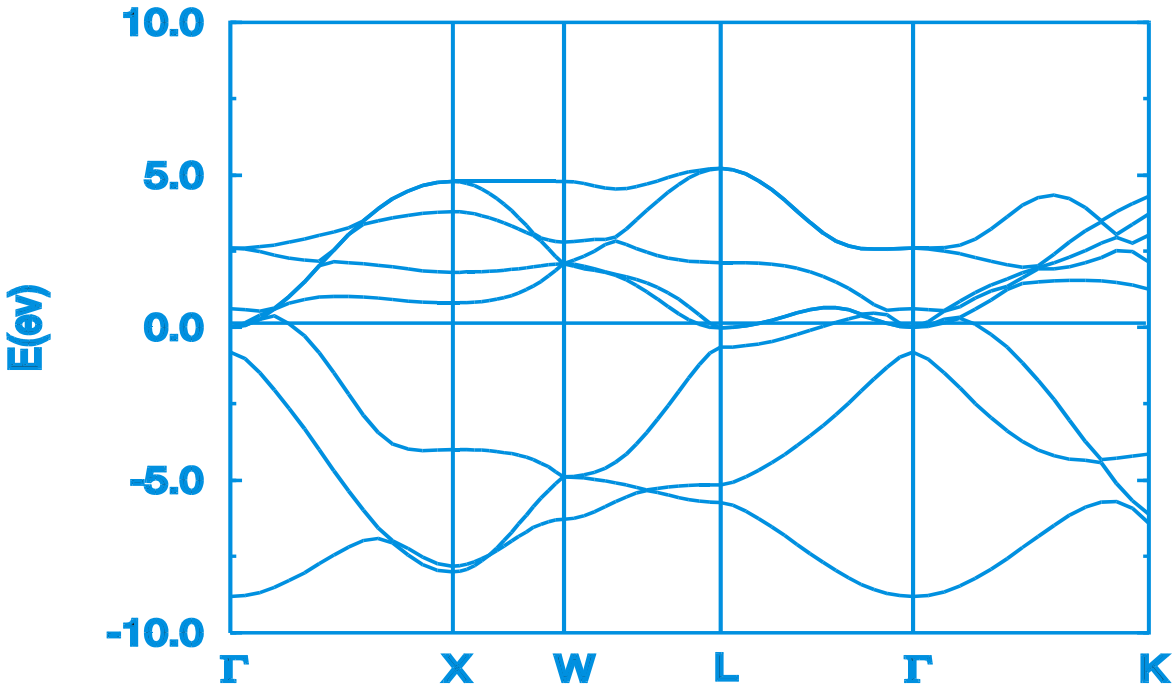

Fig. VI.14: Band structure of LaH_3 obtained by Ng et al [13] within the so-called Local Density Approximation (LDA). There is no energy gap and consequently LaH_3 is expected to be a metal

In the next sections we discuss two possibilities to open an energy gap in the band structure of a metal: the Peierls transition and electron-electron correlation effects.

VI.5 OPENING OF A GAP THROUGH A LATTICE MODULATION (PEIERLS TRANSITION)

We illustrate here with a simple linear chain of N atoms the role of a modulation in the atomic spacing on the electronic states. We consider the linear chain in Fig. VI.15. The smallest building block of this chain contains now **two** atoms instead of **one** in the equidistant case where the atoms are separated by a distance a. Consequently the Brillouin zone has boundaries at $-\frac{\pi}{b+c}$ and $+\frac{\pi}{b+c}$. This Brillouin zone is thus two times smaller (if we keep b+c=2a) than the Brillouin zone of the equidistant chain. Each band contains only N Bloch states instead of 2N in the equidistant case.

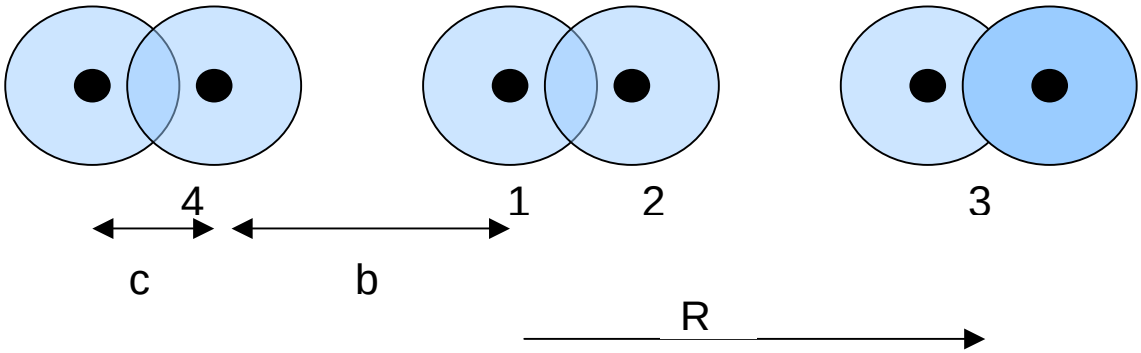

Fig. VI.15: A linear chain of non-equidistant atoms. The building block is specified by its position R. In the treatment given below we consider only the overlap integrals between atoms 1 and 2, 2 and 3, and 1 and 4.

The one-electron Schrödinger equation for the linear chain considered here is

$$H\Psi_{\mathbf{k}}(\mathbf{r}) = (T + V_1 + V_2 + h)\Psi_{\mathbf{k}}(\mathbf{r}) = E_{\mathbf{k}}\Psi_{\mathbf{k}}(\mathbf{r}) \qquad (\text{VI.21}$$

where T is the kinetic energy operator and V_i are the atomic potential of atom i in the building block with R=0. We seek a solution as a combination of atomic wave functions $\varphi_j(\mathbf{r}-\mathbf{R})$ located at the position of the atoms and satisfying the atomic Schrödinger equation

$$(T + V_1)\varphi_1 = E_{atom}\varphi_1 \quad \text{and} \quad (T + V_2)\varphi_2 = E_{atom}\varphi_2 \qquad (\text{VI.22}$$

We seek a solution of Eq.VI.21 in the form

$$\Psi_{\mathbf{k}}(\mathbf{r}) = \sum_{\mathbf{R}} e^{i\mathbf{k}\cdot\mathbf{R}}\left(\alpha\varphi_1(\mathbf{r}-\mathbf{R}) + \beta\varphi_2(\mathbf{r}-(\mathbf{R}+\mathbf{c}))\right) \qquad (\text{VI.23}$$

In the spirit of the tight-binding approximation we consider

$$\begin{aligned}&\langle\Psi_{\mathbf{k}}(\mathbf{r})|H|\varphi_1\rangle = \langle\Psi_{\mathbf{k}}(\mathbf{r})|T + V_1 + V_2 + h|\varphi_1\rangle = \\ &= \sum_{\mathbf{R}} e^{-i\mathbf{k}\cdot\mathbf{R}}\langle\alpha\varphi_1(\mathbf{r}-\mathbf{R}) + \beta\varphi_2(\mathbf{r}-(\mathbf{R}+\mathbf{c}))|T + V_1 + V_2 + h|\varphi_1\rangle = E_{\mathbf{k}}\alpha\end{aligned} \qquad (\text{VI.24}$$

and

$$\left\langle \Psi_{\mathbf{k}}(\mathbf{r})\middle|H\middle|\varphi_2\right\rangle = \left\langle \Psi_{\mathbf{k}}(\mathbf{r})\middle|T+V_1+V_2+h\middle|\varphi_2\right\rangle = \\ = \sum_{\mathbf{R}} e^{-i\mathbf{k}\cdot\mathbf{R}}\left\langle \alpha\varphi_1(\mathbf{r}-\mathbf{R})+\beta\varphi_2(\mathbf{r}-(\mathbf{R}+\mathbf{c}))\middle|T+V_1+V_2+h\middle|\varphi_2\right\rangle = E_{\mathbf{k}}\beta \qquad (\text{VI.25}$$

Keeping only nearest-neighbour terms these two equations lead to

$$\alpha(E_{atomic}-V)+\beta\left[-t_c-t_b e^{-ik(b+c)}\right]=E_k\alpha \qquad (\text{VI.26}$$

and

$$\alpha\left[-t_c-t_b e^{+ik(b+c)}\right]+\beta(E_{atomic}-V)=E_k\beta \qquad (\text{VI.27}$$

with

$$\left\langle \varphi_2\middle|V_1+h_1\middle|\varphi_2\right\rangle = -V \qquad (\text{VI.28}$$

$$\left\langle \varphi_1\middle|V_1+h_1\middle|\varphi_2\right\rangle = -t_c \qquad (\text{VI.29}$$

$$\left\langle \varphi_3\middle|V_1+h_1\middle|\varphi_2\right\rangle = -t_b \qquad (\text{VI.30}$$

A non-trivial solution exists only when the determinant vanishes, i.e.

$$(E_{atomic}-V-E_k)^2-\left[-t_c-t_b e^{-ik(b+c)}\right]\left[-t_c-t_b e^{+ik(b+c)}\right]=0 \qquad (\text{VI.31}$$

There are two solutions

$$E_k = E_{atomic}-V\pm\sqrt{t_c^2+t_b^2+2t_c t_b\cos\left[k(b+c)\right]} = \\ E_{atomic}-V\pm\sqrt{t_c^2+t_b^2+2t_c t_b\cos(2ka)} \qquad (\text{VI.32}$$

Assuming that b is not very different from c we can write

$$t_b = t(1-\delta) \quad \text{and} \quad t_c = t(1+\delta) \qquad (\text{VI.33}$$

Then

$$E_k = E_{atomic} - V \pm 2t\sqrt{\cos^2(ka) + \delta^2 \sin^2(ka)} \qquad \text{(VI.34}$$

In the limit δ=0 we obtain the electronic band structure of the equidistant linear chain but represented within a Brillouin zone that is two times too small.

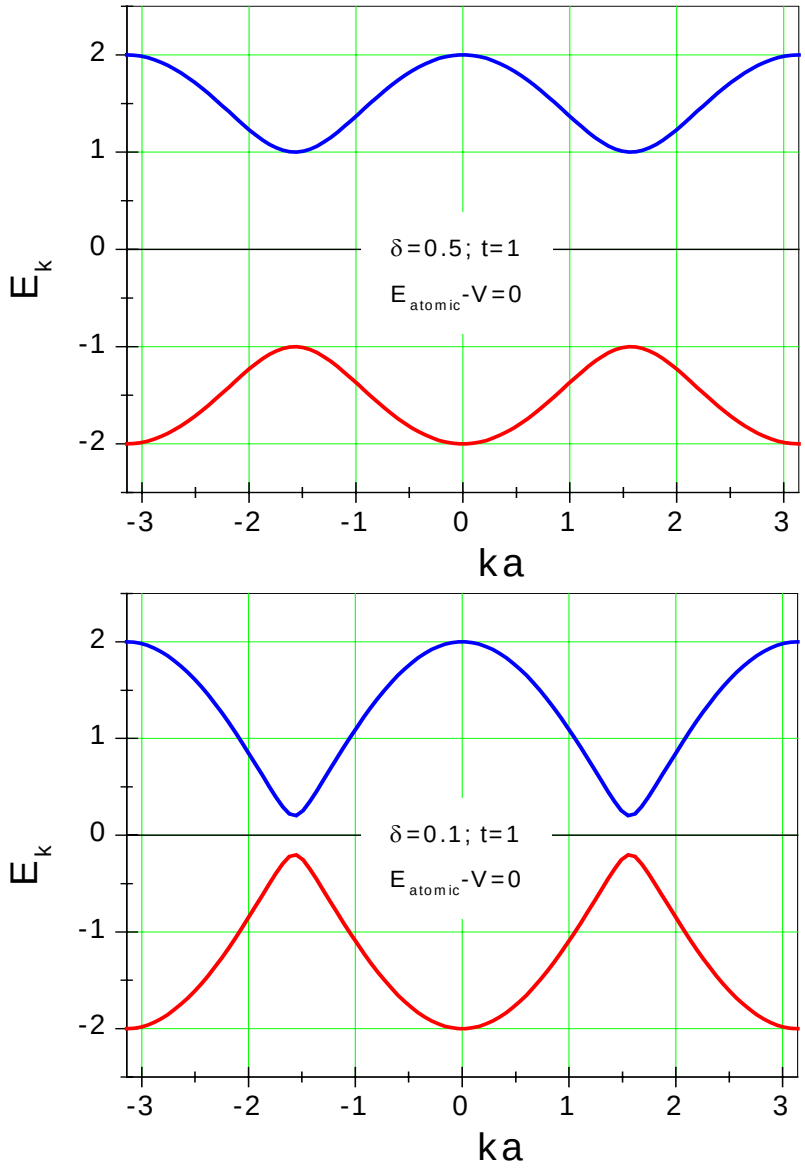

Fig. VI.16: Electron band structure of the modulated linear chain of atoms for two values of the asymmetry parameter δ. For both calculation we have taken t=1 in Eq.VI.33. For the top panel this implies that t_b=0.5 and t_c=1.5 since δ=0.5 . For the bottom panel, with δ=0.1 the corresponding values are t_b=0.9 and t_c=1.1. The gap varies linearly with δ since at the Brillouin zone boundary the cos-term in Eq.VI.33 vanishes.

An opening of the gap via a lowering of the crystal structure symmetry has been demonstrated by Kelly et al.[22]. Experimental evidence for such a low-symmetry structure in YH_3 has, however, not been found.

VI.6 ELECTRON-ELECTRON CORRELATION EFFECTS

In the last few years there has been a growing effort to understand the electronic structure of metal-hydrides with switchable properties such as YH_x and LaH_x. The interesting question is whether "traditional" one-electron band structure calculations described so far miss an essential ingredient. Or, put differently, whether strong electron correlation effects need to be invoked to reproduce the metal-insulator transition observed in these new materials. We show now how electron correlation effects can affect drastically our picture about the electronic structure of a hydride and which profound implications it may have for the nature (metallic or insulator) of the metal-hydride under consideration.

In the tight-binding approximation we discussed the electronic structure of a system on the basis of a one-electron picture. Although most features of published calculations could be understood in this way, it does of course not necessarily mean that the TBA is a good description of real metal-hydride systems since band structure calculations are essentially still based on a one-electron picture.

The next improvement is the so-called **independent electron approximation**, in which the wave function in the Schrödinger equation

$$H\Psi_{\mathbf{k}}(\mathbf{r}) = E_{\mathbf{k}}\Psi_{\mathbf{k}} \qquad (\text{VI.35}$$

is seeked in the form of a Slater determinant

$$\Psi_{\mathbf{k}}(\mathbf{r_1}\sigma_1,\mathbf{r_2}\sigma_2,.....,\mathbf{r}_N\sigma_N) = \frac{1}{\sqrt{N}}\begin{vmatrix} \varphi_1(\mathbf{r}_1,\sigma_1) & \cdots & \varphi_1(\mathbf{r}_N,\sigma_N) \\ \vdots & \ddots & \vdots \\ \varphi_N(\mathbf{r}_1,\sigma_1) & \cdots & \varphi_N(\mathbf{r}_N,\sigma_N) \end{vmatrix} \qquad (\text{VI.36}$$

which guarantees the antisymmetry of the total wave function of the system of N electrons with respect to permutations. Using Slater determinants one can then ask which sets of one-electron wave functions $\varphi_j(\mathbf{r}_i,\sigma_i)$ leads to the best approximation for the ground state energy. The best solution must satisfy the condition of stationarity

$$\delta\left(\frac{\langle\Psi_{\mathbf{k}}(\mathbf{r})|H|\Psi_{\mathbf{k}}(\mathbf{r})\rangle}{\langle\Psi_{\mathbf{k}}(\mathbf{r})|\Psi_{\mathbf{k}}(\mathbf{r})\rangle}\right)=0 \qquad \text{(VI.37}$$

and this leads to the well-known Hartree-Fock equations. These equations are certainly not the exact solution of the N-electron Schrödinger equation as they do not take into account any electron correlation effects. In fact in this approximation the electron interacts with all other electrons in such a way that first their average location is calculated and then their mutual interaction. It does, therefore, not consider the effect of the Coulomb interaction between electrons at their **actual** positions in real space.

The purpose of this section is to discuss electron correlation effects on the basis of the simplest possible systems: the negative H^- ion, the He atom and a diatomic MH-molecule. All three systems have in common that they contain two electrons, but as we shall see they make it possible to discuss specific aspects of correlation. Furthermore, the H^- ion became most relevant for the switchable metal-hydrides since Ng et al. and Eder et al. proposed their strong electron correlation models for the switchable mirrors.

VI.6.1 THE H^- ION.

The H^- ion is remarkable as it demonstrates that **one** proton is able to bind **two** electrons. Of course the binding of the second electron is not strong. This is immediately seen in the ionisation energy of the second electron which is 0.7 eV compared to 13.6 eV for the electron in a neutral hydrogen atom. To gain insight with a minimum effort of computation we follow the treatment proposed by Bethe[23] using a method developed by Hylleraas[24]. Both are based on a variational method in which one seeks a two-electron trial wave function $\Psi(\mathbf{r}_1, \mathbf{r}_2)$ which gives the lowest energy for the ground state. As in all variational approaches the calculated energy is always an upper bound of the true ground state energy and the success of the approach depends therefore strongly on the judicious choice of a class of functions for $\Psi(\mathbf{r}_1, \mathbf{r}_2)$. The ground state being isotropic the wave function depends only on the length of $\mathbf{r}_1$ and $\mathbf{r}_2$ and the angle between these two vectors. Although this is correct it leads to cumbersome calculations and is not appropriate for the treatment of Coulomb interaction which depends on the distance r_{12} between the two electrons. As proposed by Hylleraas it is much better to write the wave function $\Psi(\mathbf{r}_1, \mathbf{r}_2)$ in terms of the distances r_1, r_2 and r_{12} which also define uniquely the triangle spanned by the vectors $\mathbf{r}_1$ and $\mathbf{r}_2$. One has thus

$$\begin{aligned}
&\Psi = \Psi(r_1, r_2, r_{12}) \\
&r_1^2 = x_1^2 + y_1^2 + z_1^2 \\
&r_2^2 = x_2^2 + y_2^2 + z_2^2 \\
&r_{12}^2 = (x_2 - x_1)^2 + (y_2 - y_1)^2 + (z_2 - z_1)^2
\end{aligned} \qquad \text{(VI.38}$$

and the Schrödinger equation

$$-\frac{\hbar^2}{2m}\Delta_1\Psi-\frac{\hbar^2}{2m}\Delta_2\Psi+\left(-\frac{Ze^2}{4\pi\varepsilon_0 r_1}-\frac{Ze^2}{4\pi\varepsilon_0 r_2}+\frac{e^2}{4\pi\varepsilon_0 r_{12}}\right)\Psi=E\Psi \qquad (\text{VI.39}$$

The nuclear charge is Z=1 for the H^- ion and Z=2 for the He atom. For simplicity we measure the energy in units of Rydbergs

$$\frac{me^4}{32\pi^2\hbar^2\varepsilon_0^2}=13.6\ eV=1\ Ryd \qquad (\text{VI.40}$$

and the lengths in units of the Bohr radius a_0

$$a_0=\frac{4\pi\varepsilon_0\hbar^2}{me^2} \qquad (\text{VI.41}$$

so that Eq.VI.39 becomes

$$\Delta_1\Psi+\Delta_2\Psi+\left(+\frac{4Z}{r_1}+\frac{4Z}{r_2}-\frac{4}{r_{12}}\right)\Psi=-E\Psi \qquad (\text{VI.42}$$

The Schrödinger equation is explicitly given by

$$\begin{aligned}&\frac{\partial^2\Psi}{\partial r_1^2}+\frac{2}{r_1}\frac{\partial\Psi}{\partial r_1}+\frac{\partial^2\Psi}{\partial r_2^2}+\frac{2}{r_2}\frac{\partial\Psi}{\partial r_2}+2\frac{\partial^2\Psi}{\partial r_{12}^2}+\frac{4}{r_{12}}\frac{\partial\Psi}{\partial r_{12}}+\\&\frac{r_1^2-r_2^2+r_{12}^2}{r_1 r_{12}}\frac{\partial^2\Psi}{\partial r_1\,\partial r_{12}}+\frac{r_2^2-r_1^2+r_{12}^2}{r_2 r_{12}}\frac{\partial^2\Psi}{\partial r_2\partial r_{12}}+\\&+\left(E+\frac{4Z}{r_1}+\frac{4Z}{r_2}-\frac{4}{r_{12}}\right)\Psi=0\end{aligned} \qquad (\text{VI.43}$$

After multiplication by $r_1r_2r_{12}$ we obtain

$$r_1 r_2 r_{12}\frac{\partial^2\Psi}{\partial r_1^2}+2r_2 r_{12}\frac{\partial\Psi}{\partial r_1}+r_1 r_2 r_{12}\frac{\partial^2\Psi}{\partial r_2^2}+2r_1 r_{12}\frac{\partial\Psi}{\partial r_2}+2r_1 r_2 r_{12}\frac{\partial^2\Psi}{\partial r_{12}^2}+4r_1 r_2\frac{\partial\Psi}{\partial r_{12}}+$$
$$\left(r_1^2-r_2^2+r_{12}^2\right)r_2\frac{\partial^2\Psi}{\partial r_1\,\partial r_{12}}+\left(r_2^2-r_1^2+r_{12}^2\right)r_1\frac{\partial^2\Psi}{\partial r_2\,\partial r_{12}}+ \qquad \text{(VI.44}$$
$$+\left(Er_1 r_2 r_{12}+4Zr_2 r_{12}+4Zr_1 r_{12}-4r_1 r_2\right)\Psi=0$$

which can be interpreted as the Euler equation of the following variational problem

$$\int_0^\infty dr_1\int_0^\infty dr_2\int_{|r_2-r_1|}^{r_1+r_2} dr_{12}\left\{\begin{array}{l} r_1 r_2 r_{12}\left[\left(\frac{\partial\Psi}{\partial r_1}\right)^2+\left(\frac{\partial\Psi}{\partial r_2}\right)^2+2\left(\frac{\partial\Psi}{\partial r_{12}}\right)^2\right] \\ \left(r_1^2-r_2^2+r_{12}^2\right)r_2\frac{\partial\Psi}{\partial r_1}\frac{\partial\Psi}{\partial r_{12}}+\left(r_2^2-r_1^2+r_{12}^2\right)r_1\frac{\partial\Psi}{\partial r_2}\frac{\partial\Psi}{\partial r_{12}} \\ -\left[4Zr_{12}\left(r_1+r_2\right)-4r_1 r_2\right]\Psi^2 \end{array}\right\}= \qquad \text{(VI.45}$$
$$=E\int_0^\infty dr_1\int_0^\infty dr_2\int_{|r_2-r_1|}^{r_1+r_2} dr_{12}\,r_1 r_2 r_{12}\Psi^2$$

where E should be a minimum. Introducing the new variables

$$\begin{aligned} s&=r_1+r_2 \\ t&=r_2-r_1 \\ u&=r_{12} \end{aligned} \qquad \text{(VI.46}$$

we obtain a more transparent form of Eq.VI.45

$$\int_0^\infty ds\int_0^s du\int_0^u dt\left\{\begin{array}{l} u\left(s^2-t^2\right)\left[\left(\frac{\partial\Psi}{\partial s}\right)^2+\left(\frac{\partial\Psi}{\partial t}\right)^2+\left(\frac{\partial\Psi}{\partial u}\right)^2\right] \\ 2s\left(u^2-t^2\right)\frac{\partial\Psi}{\partial s}\frac{\partial\Psi}{\partial u}+2t\left(s^2-u^2\right)_1\frac{\partial\Psi}{\partial t}\frac{\partial\Psi}{\partial u} \\ -\left(4Zsu-\left(s^2-t^2\right)\right)\Psi^2 \end{array}\right\}= \qquad \text{(VI.47}$$
$$=\frac{1}{2}E\int_0^\infty ds\int_0^s du\int_0^u dt\left[u\left(s^2-t^2\right)\right]\Psi^2$$

Independent electrons

The first and simplest approximation is that of independent electrons. In the spirit of this approach it is reasonable to write the wave function as the product of two hydrogenic wave functions, i.e.

$$\Psi = \Psi(r_1, r_2, r_{12}) = \Psi(r_1 + r_2) = Ae^{-a(r_1+r_2)} = Ae^{-as} \qquad \text{(VI.48}$$

Then Eq.VI.47 takes the much simpler form

$$\int_0^\infty ds \int_0^s du \int_0^u dt \begin{Bmatrix} u(s^2 - t^2)\left(\frac{\partial \Psi}{\partial s}\right)^2 \\ -\left(4Zsu - (s^2 - t^2)\right)\Psi^2 \end{Bmatrix} = \qquad \text{(VI.49}$$

$$= \frac{1}{2} E \int_0^\infty ds \int_0^s du \int_0^u dt \left[u(s^2 - t^2)\right]\Psi^2$$

Introducing the trial function Eq.VI.48 into Eq.VI.49 leads to an expression of the form

$$E = \frac{a^2 I_5 + kI_4}{\frac{1}{2} I_5} \qquad \text{(VI.50}$$

with $I_n(a) = \int_0^\infty s^n e^{-2as} ds$ and $k = \frac{25}{16} - 5Z$. From the stationarity condition (similar to Eq.VI.37)

$$\frac{\partial E}{\partial a} = \frac{\partial}{\partial a}\left(\frac{a^2 I_5 + kI_4}{\frac{1}{2} I_5}\right) = 0 \qquad \text{(VI.51}$$

noting that

$$I_4 = \frac{2a}{5} I_5$$
$$\frac{\partial I_5}{\partial a} = \frac{-6}{a} I_5 \qquad \text{(VI.52}$$

we obtain that

$$a = Z - \frac{5}{16} \qquad \text{(VI.53}$$

and, consequently, the wave function

$$\Psi = Ae^{-\left(Z-5/16\right)s} = Ae^{-\left(Z-5/16\right)r_1}e^{-\left(Z-5/16\right)r_2} \qquad \text{(VI.54}$$

and the energy of the two electron system

$$E = -2\left(Z - 5/16\right)^2 \qquad \text{(VI.55}$$

These results have a simple interpretation: the two electrons are partially screening the attractive Coulomb potential of the nucleus. There common radius is therefore larger than the radius one would expect for a single electron. The two electrons behave as if the charge of the nucleus would be reduced by 5/16. For the specific case of the H^- ion

$$a = 1 - \frac{5}{16} = \frac{11}{16} \qquad \text{(VI.56}$$

and

$$E = -2\left(1 - 5/16\right)^2 = -\frac{121}{128} = -0.94531 \qquad \text{(VI.57}$$

instead of the exact value -1.056. In real units this corresponds to a common orbit radius

$$r_{common} = \frac{16}{11} \times 0.0529\ \text{nm} = 0.077\ \text{nm} \qquad \text{(VI.58}$$

and an energy

$$E_0 = -2\left(1 - \frac{5}{16}\right)^2 \times 13.6\ eV = -12.86\ eV \qquad \text{(VI.59}$$

which is less negative than the energy of a system consisting of a neutral H-atom (-13.6 eV) and an electron at infinite distance from the proton. This implies that the trial function in Eq.VI.48 is not good enough to stabilise the H^- ion for which exact calculations and experiments show that E=-14.36 eV. The result in Eq.VI.59 is, therefore, wrong by approximately 1.4 eV. It is important to note here that for the He atom, there are however no problems. The calculated energy

$$E = -2\left(2 - 5/16\right)^2 = -\frac{729}{128} = -5.69531 \qquad \text{(VI.60}$$

is quite close to the exact result of 5.807. The variational value -77.46 eV being much more negative than that of a He^+ ion and an electron at infinite distance (-54.4 eV) the He atom is found to be stable. We see therefore, that a method which works very well for the He atom fails completely for the H^- ion ! The question is then how to improve our trial function in order to obtain a better estimate of the ground state energy of the H^- ion. As Chandrasekhar[25] we shall proceed in two steps.

Improved screening

First we improve the screening by allowing explicitly that the two electrons are not the same orbit, but that one electron is essentially screening the proton potential so that the second electron moves on a much larger orbit. The wave function is then chosen to be of the form

$$\Psi = e^{-ar_1}e^{-br_2} + e^{-ar_2}e^{-br_1} \qquad \text{(VI.61}$$

which can be written in terms of the variable t, u and s defined in Eq.VI.46 as

$$\Psi = e^{-\alpha s}\cosh(\beta t) \qquad \text{(VI.62}$$

Introducing this expression into Eq.VI.47 one finds that a =1.03925 and b =0.28309 lead to the minimum for the energy, E_1=-1.0266. This value corresponds to E_1=-13.96 eV which is now more negative (by 0.36 eV) than the ground state of the neutral H-atom. The H^- ion is thus stable. It consists of an inner electron moving on an orbit with a radius

$$r_{in} = \frac{0.0529\,\text{nm}}{1.03925} = 0.0509\,\text{nm} \qquad \text{(VI.63}$$

and an outer electron on an orbit of radius

$$r_{out} = \frac{0.0529\,\text{nm}}{0.28309} = 0.1869\,\text{nm} \qquad \text{(VI.64}$$

In this approach the inner electron is slightly pushed towards the nucleus (note that 0.0509 nm is slightly smaller than 0.0529 nm for the hydrogen atom) while the second one is very far from the nucleus. The H^- ion has then a radius which is 3.532 times larger than that of a neutral H atom.

Electron correlation

The second improvement of the trial function is to take into account that electrons experience a mutually repulsive interaction and that they try to avoid each other. To provide for the effect of electron correlation in space we choose a trial wave function of the form

$$\Psi = \left(e^{-ar_1}e^{-br_2} + e^{-ar_2}e^{-br_1}\right)\left(1 + cr_{12}\right) \qquad \text{(VI.65}$$

or in the s, t, u variables

$$\Psi = e^{-\alpha s}\, cosh\left(\beta t\right)\left(1 + cu\right) \qquad \text{(VI.66}$$

With such a function Chandrasekhar obtained a = 1.07478, b = 0.47758 and c = 0.31214 which lead to the energy E_2 = -1.0518, i.e. -14.31 eV in remarkable agreement with the exact result -14.36 eV. The values of a, b and c lead to

$$r_{in} = 0.9304\, a_0 = 0.0492\ \text{nm} \qquad \text{(VI.67}$$

$$r_{out} = 2.094\, a_0 = 0.1108\ \text{nm} \qquad \text{(VI.68}$$

$$r_{corr.} = 3.204\, a_0 = 0.170\ \text{nm} \qquad \text{(VI.69}$$

and to a wave function

$$\Psi = \left(e^{-r_1/r_{in}}e^{-r_2/r_{out}} + e^{-r_2/r_{in}}e^{-r_1/r_{out}}\right)\left(1 + \frac{r_{12}}{r_{corr.}}\right) \qquad \text{(VI.70}$$

As expected the introduction of correlation reduces the calculated size of the H^- ion, as the electrons are avoiding each through the term $(1+r_{12}/r_{corr.})$.This leads to a so-called correlation hole which is visible in Fig. VI.17. In this figure, the probability $|\Psi(\mathbf{r}_1, \mathbf{r}_2)|^2$ is plotted as a function of $\mathbf{r}_1 = (x_1, x_2)$ for chosen values $\mathbf{r_2} = (x_2, 0)$ of electron 2. As an illustration we have chosen x_2= -0.05, 0.05, 0.1 and 0.15 nm. The clear depression of the wave function amplitude of electron 1 near the position of electron 2 is due to the correlation term $(1+r_{12}/r_{corr.})$.

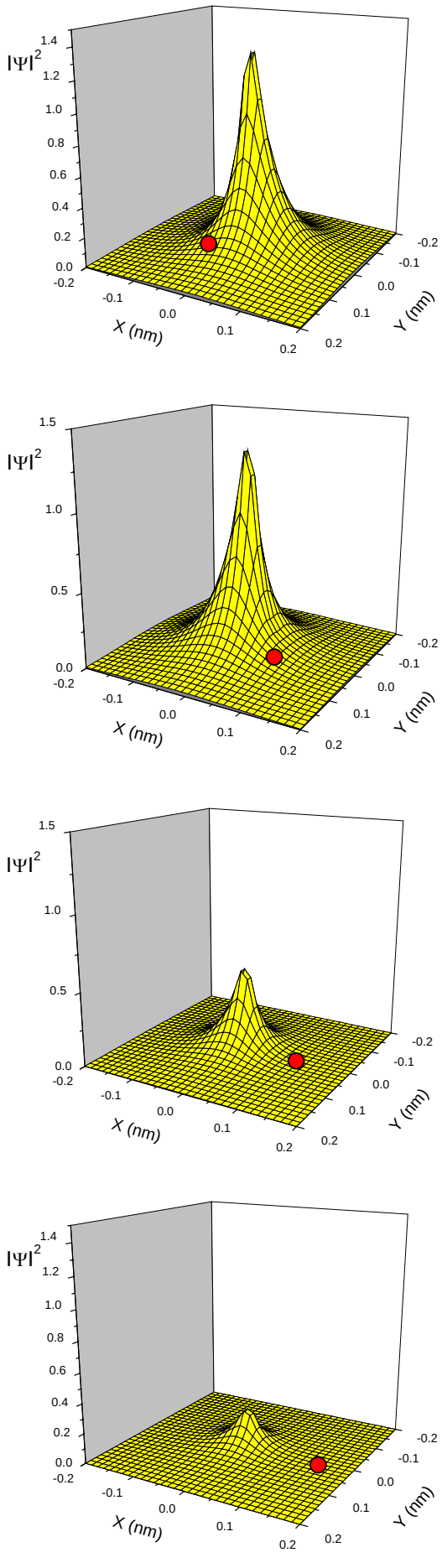

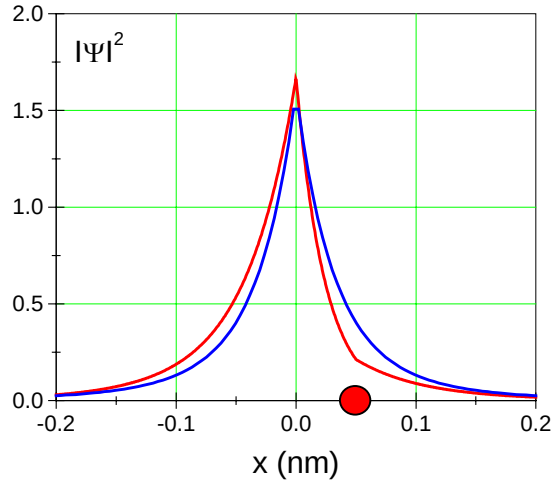

Fig. VI.17: Probability to find electron 1 of the H^- ion (Eq.VI.62) for fixed values of the position of electron 2. For the illustration the position of electron 2 is taken, from top to bottom, at -0.05, 0.05, 0.1 and 0.15 nm on the x-axis. These positions are indicated with a red dot. There is a clear correlation between the two electrons, as electron 1 tends to avoid electron 2. This especially clear in the right panel for the case where the position of electron 2 is taken at 0.05. The red curve corresponds to Eq.VI.70 while the blue curve corresponds to Eq.VI.61 (without electron correlation).

VI.6.2 ENERGY GAP DUE TO ELECTRON CORRELATION

How do the considerations given above about electron correlation lead to the formation of an electronic gap in YH_3 ? To answer this question it is useful to consider a simple chain of hydrogen atoms. According to standard one-electron band theory this should be a metal since each hydrogen contributes only one electron and consequently the band is half-full. However, we have seen in the H^- ion problem that the two-electron state has an energy that is 12.9 eV higher than that of the one-electron ground state. The Hubbard electron-electron interaction energy U_H is thus especially large and it costs a lot of energy (in fact U_H) to move one electron from atom i to atom i+1. Once this energy is paid the electron can move freely to the right as a Bloch electron. Similarly, the hole left at site i can move freely to the left. This is schematically illustrated in Fig. VI.18. The band for the moving electron is called the **upper Hubbard band**. That for the hole is the **lower Hubbard band**. These two bands correspond, respectively, to the (N+1)-state (electron addition spectrum as measured in inverse photoemission) and the (N-1)-state (electron removal spectrum as measured in photoemission) state of the system.

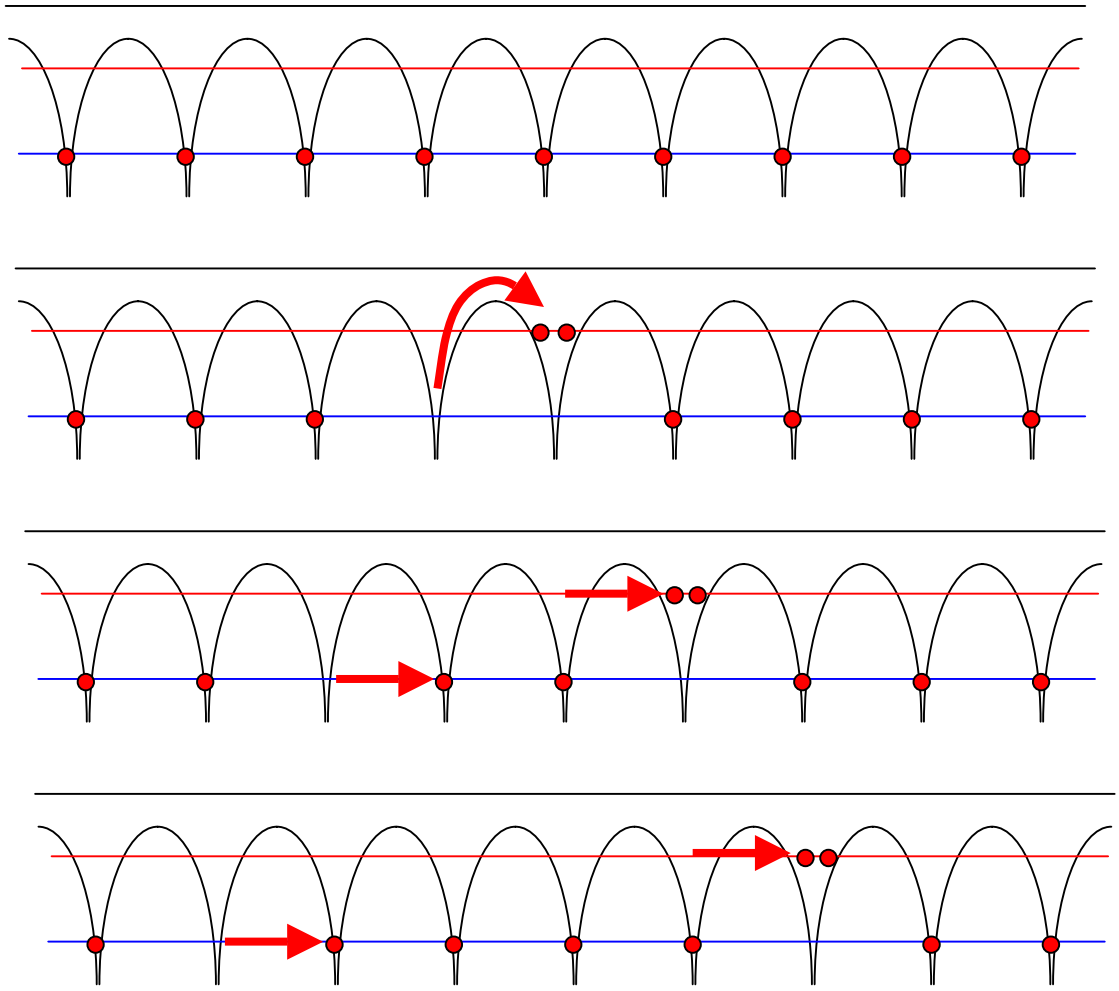

Fig. VI.18: Movement of an electron and a hole in a linear chain of hydrogen atoms in presence of electron correlation. The system is a semiconductor with a gap equal to U_H. Note that the movement of the hole and electron are not correlated.

In YH_3 the situation is somewhat more complicated since the hopping of the electron (hole) between two hydrogen atoms is happening via the intermediate yttrium atom.
Correlation effects forces us to find a new way to describe the state of a many-electron system. Instead of the density of states used so far one introduces the concept of electron-addition spectrum and electron-removal spectrum. This is easily illustrated with the linear chain of N hydrogen atoms. If one adds an extra electron, this electron needs to be added locally to one of the neutral H to form a negative H^- ion. The energy of this two-electron system is U_H higher than that of the ground state. There are N possibilities to add an extra electron and therefore the addition spectrum contains N states. There are evidently also N possibilities to remove an electron. Therefore the electron removal spectrum contains also N states. Note that this reasoning is possible because we assume that the band width W_B of each Hubbard band is much smaller than the electron correlation energy U_H. This is illustrated in Fig. VI.19.

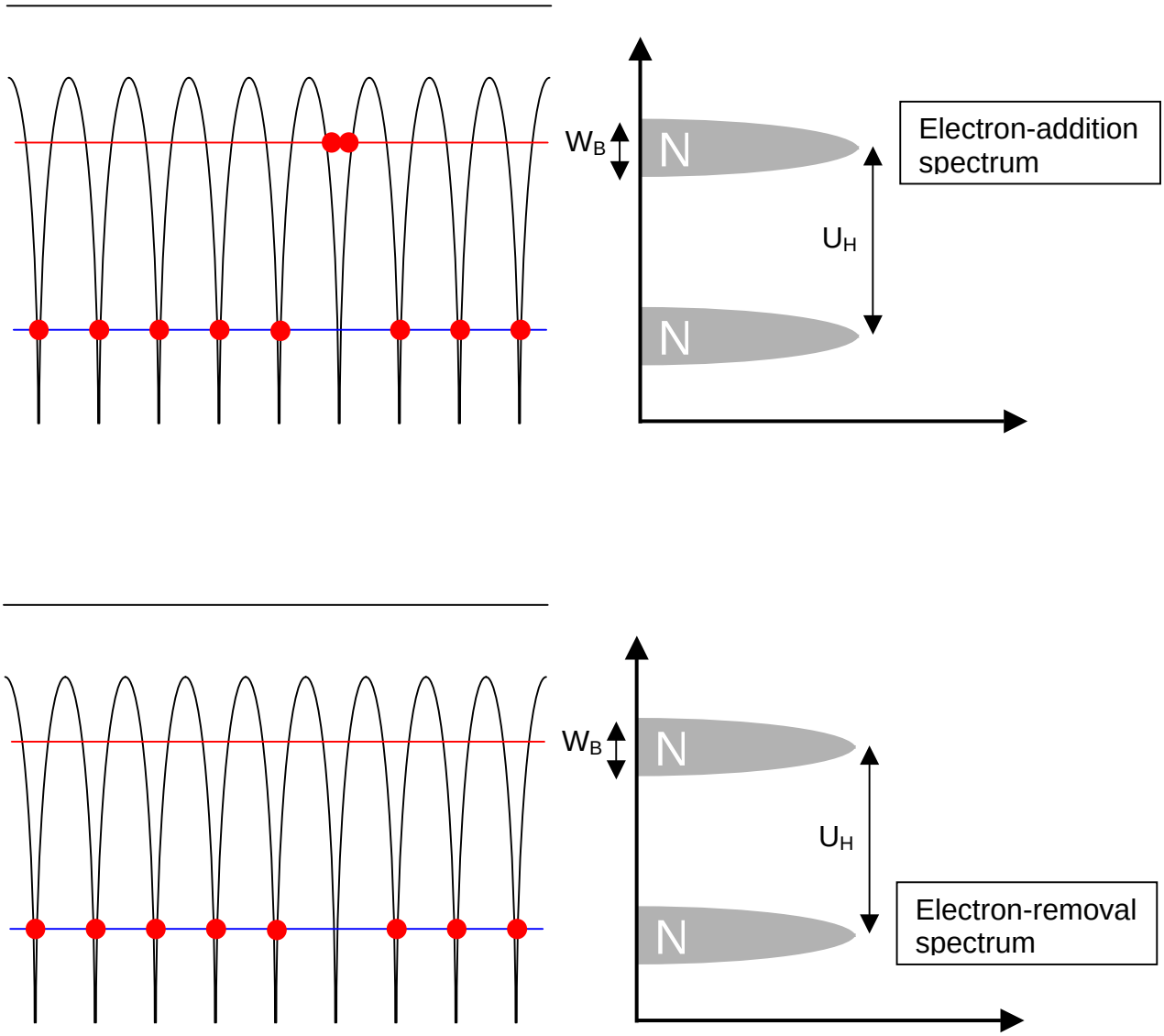

Fig. VI.19: Definition of the electron-addition and electron-removal spectra for a linear chain of hydrogen atoms. The Hubbard correlation energy is assumed to be much larger than the bandwidth.

We consider now the influence of doping with electrons. For this we assume that one of the hydrogen atoms has been replaced by an impurity atom with two electrons. To keep every thing simple we assume that this is done without changing the periodic potential. Then this impurity has its two electrons in a two-electron state with the same energy as that of the two-electron state in a H^- ion. There are then only N-1 possibilities to add an extra electron to this electron doped chain. The electron-removal spectrum contains only N-1 states in the lower Hubbard band, and of course, the two states corresponding to the two electrons on the impurity. The Fermi energy lies just between the upper Hubbard band and the two-electron impurity state.
For hole doping we have a similar situation. An electron can only be removed from N-1 sites. On the other hand an electron can be added at N-1 sites which are already occupied by one electron, and, in addition, one electron with spin up or and electron with spin-down can be added to the impurity site. For each of these electrons the energy is just above the lower Hubbard band. The Fermi energy lies in-between since the states with the N-1 electrons are occupied but not the impurity states (by definition since the impurity is hole doping the chain !). This is shown in Fig. VI.20.

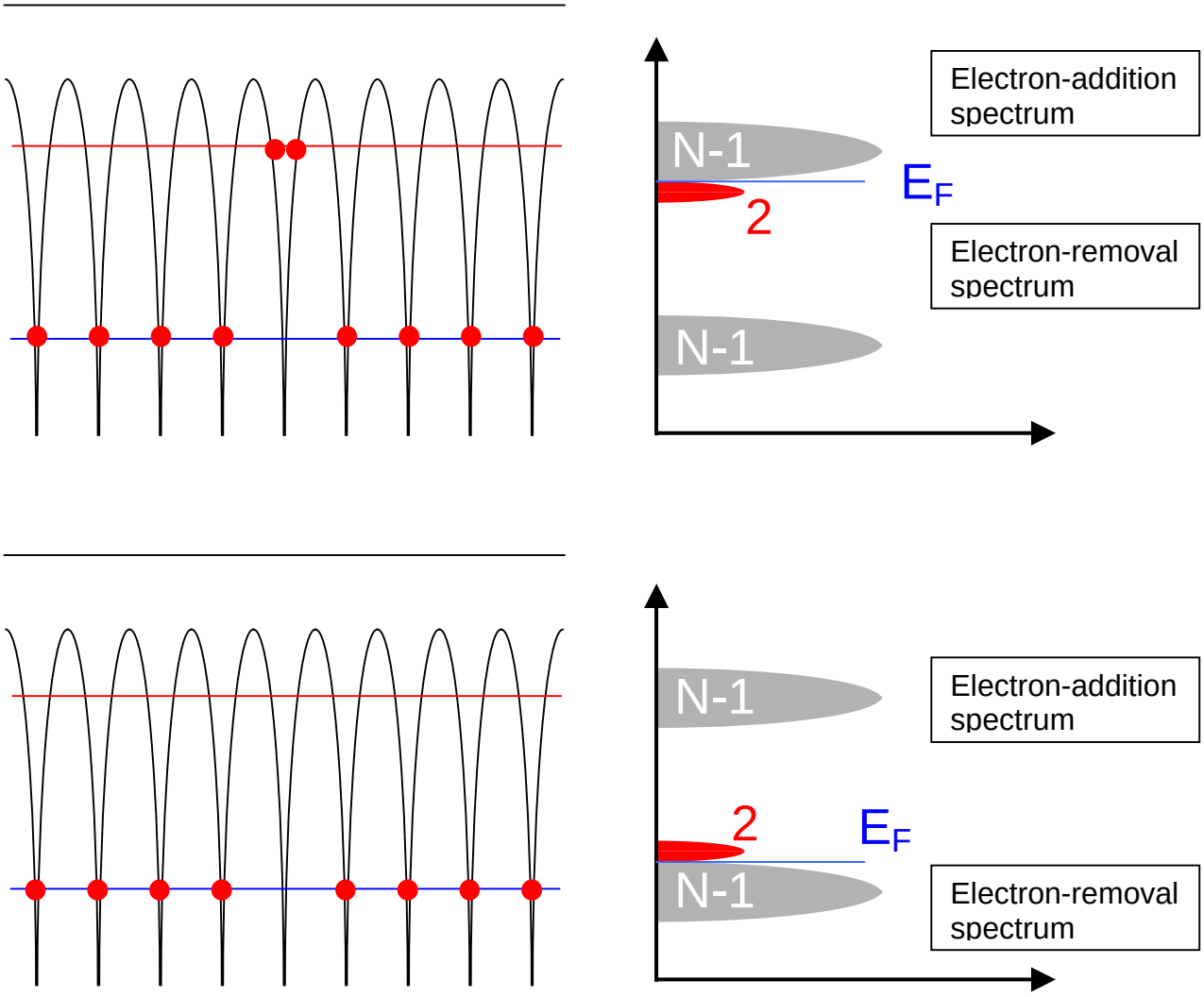

Fig. VI.20: Electron-removal and electron-addition spectra for the linear chain of hydrogen atoms with electron doping and hole doping.

So far we considered only one impurity. If we have x impurities then we obtain the spectral weight transfer shown in Fig. VI.21. This is in sharp contrast with what happens in a conventional semiconductor. In a semiconductor both the valence band and the conduction band contain 2N states. When x electron are doped they occupy x states in the conduction band. The electron removal spectrum consists thus of x states (from the conduction band) and 2N states from the valence band. The electron-addition spectrum has 2N-x states in the conduction band.

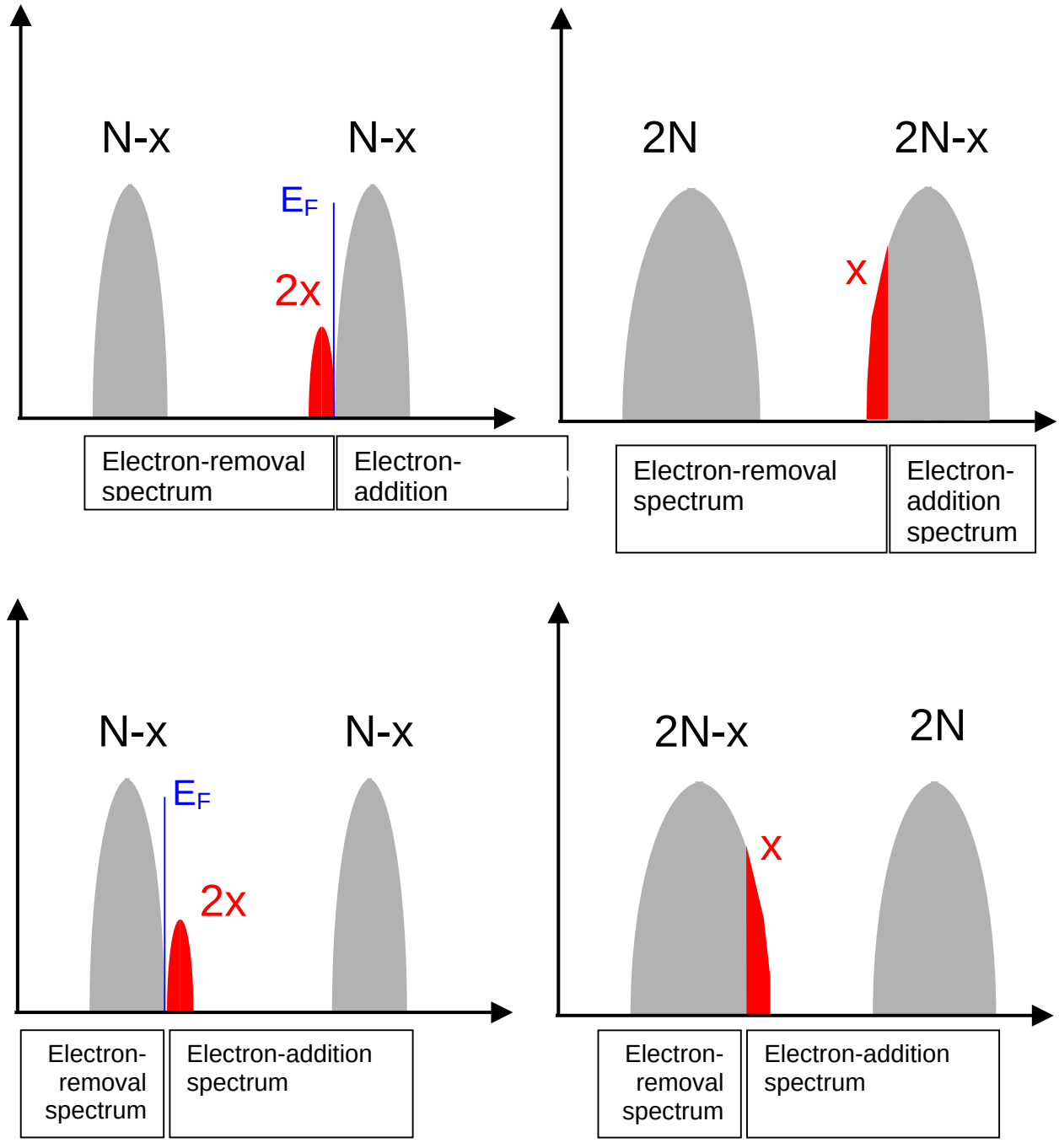

Fig. VI.21: Spectral weight transfer in a Hubbard system (left) and a classical semiconductor (right) for electron doping (top) and hole doping (bottom) with x impurities[26].

VI.6.3 THE DIATOMIC MOLECULE.

The simplest example of a system of strongly correlated electrons not centred on the same nucleus consists of a diatomic molecule with two electrons in the orbitals $\varphi_s(\mathbf{r}_i-\mathbf{R}_s)$ and $\varphi_d(\mathbf{r}_i-\mathbf{R}_d)$ which shall be denoted below as s_i and d_i. The situation we have in mind is that of a diatomic molecule consisting of a hydrogen atom and a transition metal with only one d-electron. To some extent this is what happens in YH_{2+x}. Two of the three electrons of Y have been lowered so much in energy that they do not need to be taken into account. What is left are hydrogen occupying octahedral sites in a lattice of effectively monovalent transition metal "atoms" M≡[YH_2]with one valence d-electron. Although this problem is very similar to that of the H_2 molecule treated in Chapter II we give here a detailed description of its solution.

The Schrödinger equation of such a molecule is

$$-\frac{\hbar^2}{2m}\Delta_1\Psi-\frac{\hbar^2}{2m}\Delta_2\Psi+\left(\begin{array}{l}-\dfrac{e^2}{4\pi\varepsilon_0|\mathbf{R}_H-\mathbf{r}_1|}-\dfrac{e^2}{4\pi\varepsilon_0|\mathbf{R}_Y-\mathbf{r}_1|}\\ -\dfrac{e^2}{4\pi\varepsilon_0|\mathbf{R}_H-r_2|}-\dfrac{e^2}{4\pi\varepsilon_0|\mathbf{R}_Y-\mathbf{r}_2|}+\dfrac{e^2}{4\pi\varepsilon_0|\mathbf{r}_2-\mathbf{r}_1|}\end{array}\right)\Psi=E\Psi \qquad (\text{VI.71}$$

where $\mathbf{R}_H$ and $\mathbf{R}_Y$ are the position vectors of the H and Y nuclei, respectively.
For simplicity we write Eq.VI.63 as

$$\left[T_1+V_Y(1)+V_H(1)+T_2+V_Y(2)+V_H(2)+V_{12}\right]\Psi=E\Psi \qquad (\text{VI.72}$$

We construct a two-electron state from the s-orbital s_i and the d-orbital d_i, the index i indicating which electron is occupying a particular orbital. There are six possible states

$$\begin{aligned}\Phi_0&=\frac{1}{\sqrt{2}}\left[d_1s_2+d_2s_1\right]\left|\uparrow\downarrow-\downarrow\uparrow\right\rangle\\ \Phi_1^1&=\frac{1}{\sqrt{2}}\left[d_1s_2-d_2s_1\right]\left|\uparrow\uparrow\right\rangle\\ \Phi_1^0&=\frac{1}{\sqrt{2}}\left[d_1s_2-d_2s_1\right]\left|\uparrow\downarrow+\downarrow\uparrow\right\rangle\\ \Phi_1^{-1}&=\frac{1}{\sqrt{2}}\left[d_1s_2-d_2s_1\right]\left|\downarrow\downarrow\right\rangle\end{aligned} \qquad (\text{VI.73}$$

$$\begin{aligned}\Phi_Y&=\left[d_1d_2\right]\left|\uparrow\downarrow-\downarrow\uparrow\right\rangle\\ \Phi_H&=\left[s_1s_2\right]\left|\uparrow\downarrow-\downarrow\uparrow\right\rangle\end{aligned} \qquad (\text{VI.74}$$

The three states Φ_0, Φ_Y, Φ_H have zero total spin while the states Φ_1^1, Φ_1^0, Φ_1^{-1} have total spin 1. The solution of the Schrödinger equation will be seeked in the form of a linear combination of these six wave functions, i.e.

$$\Psi = c_0\Phi_0 + c_1\Phi_1^1 + c_2\Phi_1^0 + c_3\Phi_1^{-1} + c_4\Phi_Y + c_5\Phi_H \qquad \text{(VI.75}$$

In building up the matrix equation for the coefficients c_i we need to calculate matrix elements of the form

$$\begin{aligned}
&\left\langle \left[d_1 s_2 \pm d_2 s_1\right] \middle| \left[d_1 s_2 \pm d_2 s_1\right] \right\rangle \\
&\left\langle \left[d_1 s_2 \pm d_2 s_1\right] \middle| d_1 d_2 \right\rangle \\
&\left\langle \left[d_1 s_2 \pm d_2 s_1\right] \middle| s_1 s_2 \right\rangle \\
&\left\langle d_1 d_2 \middle| s_1 s_2 \right\rangle
\end{aligned} \qquad \text{(VI.76}$$

and

$$\begin{aligned}
&\left\langle \left[d_1 s_2 \pm d_2 s_1\right] \middle| H \middle| \left[d_1 s_2 \pm d_2 s_1\right] \right\rangle \\
&\left\langle \left[d_1 s_2 \pm d_2 s_1\right] \middle| H \middle| d_1 d_2 \right\rangle \\
&\left\langle \left[d_1 s_2 \pm d_2 s_1\right] \middle| H \middle| s_1 s_2 \right\rangle
\end{aligned} \qquad \text{(VI.77}$$

As in the TBA we assume that the overlaps between s and d orbitals are such that

$$\left\langle s_1 \middle| d_1 \right\rangle = \left\langle s_2 \middle| d_2 \right\rangle = 0 \qquad \text{(VI.78}$$

On the basis of what we have learned with the H^--ion and the He atom we assume that correlation effects are not important for the yttrium d-orbital (because of the large size of Y) but that they must be included for the hydrogen s-orbital. This means that the Coulomb repulsion is introduced in our model only when the two electrons are on hydrogen and not when they are on the yttrium. This implies that

$$\begin{aligned}
&\left\langle d_1 d_2 \middle| V_{12} \middle| d_1 d_2 \right\rangle \cong 0 \\
&\left\langle s_1 s_2 \middle| V_{12} \middle| s_1 s_2 \right\rangle = U
\end{aligned} \qquad \text{(VI.79}$$

Introducing the notation

$$\left[T_i + V_Y(i)\right]d_i = \varepsilon_Y^0 d_i$$
$$\left[T_i + V_H(i)\right]s_i = \varepsilon_H^0 s_i \qquad \text{(VI.80}$$

$$\varepsilon_Y = \varepsilon_Y^0 + \left\langle d_i \left| V_H(i) \right| d_i \right\rangle$$
$$\varepsilon_H = \varepsilon_H^0 + \left\langle s_i \left| V_Y(i) \right| s_i \right\rangle$$

$$W_Y = \left\langle d_i \left| V_Y(i) \right| s_i \right\rangle$$
$$W_H = \left\langle d_i \left| V_H(i) \right| s_i \right\rangle \qquad \text{(VI.81}$$
$$U_H = \left\langle s_1 s_2 \left| V_{12} \right| s_1 s_2 \right\rangle$$

we obtain the following matrix

$$\begin{pmatrix} (\varepsilon_Y + \varepsilon_H) & 0 & 0 & 0 & \sqrt{2}W_Y & \sqrt{2}W_H \\ 0 & (\varepsilon_Y + \varepsilon_H) & 0 & 0 & 0 & 0 \\ 0 & 0 & (\varepsilon_Y + \varepsilon_H) & 0 & 0 & 0 \\ 0 & 0 & 0 & (\varepsilon_Y + \varepsilon_H) & 0 & 0 \\ \sqrt{2}W_Y & 0 & 0 & 0 & (2\varepsilon_Y) & 0 \\ \sqrt{2}W_H & 0 & 0 & 0 & 0 & (2\varepsilon_H + U_H) \end{pmatrix} \begin{pmatrix} c_0 \\ c_1 \\ c_2 \\ c_3 \\ c_4 \\ c_5 \end{pmatrix} = E \begin{pmatrix} c_0 \\ c_1 \\ c_2 \\ c_3 \\ c_4 \\ c_5 \end{pmatrix} \qquad \text{(VI.82}$$

There exists a non trivial solution if the following determinant vanishes,

$$\begin{vmatrix} (\varepsilon_Y + \varepsilon_H) - E & 0 & 0 & 0 & \sqrt{2}W_Y & \sqrt{2}W_H \\ 0 & (\varepsilon_Y + \varepsilon_H) - E & 0 & 0 & 0 & 0 \\ 0 & 0 & (\varepsilon_Y + \varepsilon_H) - E & 0 & 0 & 0 \\ 0 & 0 & 0 & (\varepsilon_Y + \varepsilon_H) - E & 0 & 0 \\ \sqrt{2}W_Y & 0 & 0 & 0 & (2\varepsilon_Y - E) & 0 \\ \sqrt{2}W_H & 0 & 0 & 0 & 0 & (2\varepsilon_H + U_H - E) \end{vmatrix} = 0$$

(VI.83

There are three degenerate states with energy

$$E = \varepsilon_Y + \varepsilon_H \qquad \text{(VI.84}$$

The other three states have an energy given by

$$\begin{vmatrix} (\varepsilon_Y + \varepsilon_H) - E & \sqrt{2}W_Y & \sqrt{2}W_H \\ \sqrt{2}W_Y & (2\varepsilon_Y - E) & 0 \\ \sqrt{2}W_H & 0 & (2\varepsilon_H + U_H - E) \end{vmatrix} = 0 \qquad (\text{VI.85}$$

For a discussion of the behaviour of the roots of this equation we do not make any difference between W_Y and W_H and take the zero of energy at ε_Y . Then,

$$\begin{vmatrix} (\varepsilon_H - E) & W & W \\ W & -E & 0 \\ W & 0 & (2\varepsilon_H + U_H - E) \end{vmatrix} = 0 \qquad (\text{VI.86}$$

with the secular equation

$$E(\varepsilon_H - E)(2\varepsilon_H + U_H - E) + W^2(2\varepsilon_H + U_H - 2E) = 0 \qquad (\text{VI.87}$$

Let us now consider the special case where the hybridisation energy is negligible, i.e. W=0. Then the energy of the three states are:

$$\begin{aligned} E_0 &= 2\varepsilon_H + U_H \\ E_1 &= \varepsilon_H \\ E_2 &= 0 \end{aligned} \qquad (\text{VI.88}$$

In addition to these three states we have also three other states which are degenerate with that of energy E_1,

$$\begin{aligned} E_3 &= \varepsilon_H \\ E_4 &= \varepsilon_H \\ E_5 &= \varepsilon_H \end{aligned} \qquad (\text{VI.89}$$

They correspond to the situations shown schematically in Fig. VI.22.

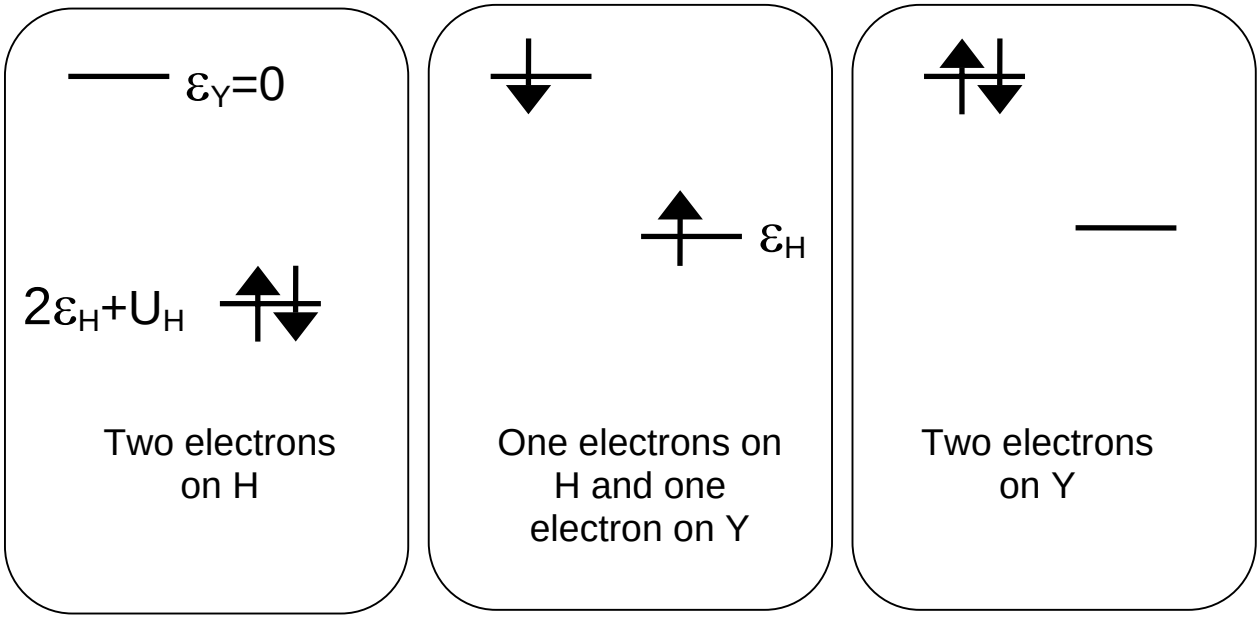

Fig. VI.22: The states corresponding to three energies of a diatomic molecule with zero hybridisation (W=0) but a finite electron-electron repulsion on the hydrogen. The four degenerate states consist of a singlet (S=0) state and a triplet (S=1) state.

Another simple situation is encountered when U_H is very large, which implies that the hydrogen orbital cannot be doubly occupied. Equation VI.87 reduces then to

$$E\left(\varepsilon_H - E\right) + W^2 = 0 \qquad \text{(VI.90}$$

with the solutions

$$E_0 = \frac{\varepsilon_H - \sqrt{\varepsilon_H^2 + 4W^2}}{2}$$
$$E_1 = \frac{\varepsilon_H + \sqrt{\varepsilon_H^2 + 4W^2}}{2} \qquad \text{(VI.91}$$

The other levels have an energy

$$E_2 = \varepsilon_H$$
$$E_3 = \varepsilon_H$$
$$E_4 = \varepsilon_H \qquad \text{(VI.92}$$
$$E_5 = \infty$$

and we have the situation indicated schematically in Fig. VI.23. The ground state has a lower energy when W is non-zero than for a situation where hybridisation vanishes. This is what we expect since W≠0 corresponds to a situation where tunnelling of an electron from the hydrogen to the yttrium (and vice versa) is possible. This weaker localisation of the electrons in space leads to a lowering of their energy. The ground state having zero total spin is non magnetic. At zero temperature only the S=0 singlet state is occupied. When temperature is increased excitation to the next level (triplet state S=1) are possible. Such excitations involve very little changes in charge distribution but change reduce the total spin from zero to 1. They are, therefore, called **spin excitations.** When the temperature is further increased the singlet-triplet splitting is not important anymore. The excitation to the top level involve predominantly charges. This separation into spin and charge excitation is a typical characteristic of strongly correlated electron systems.

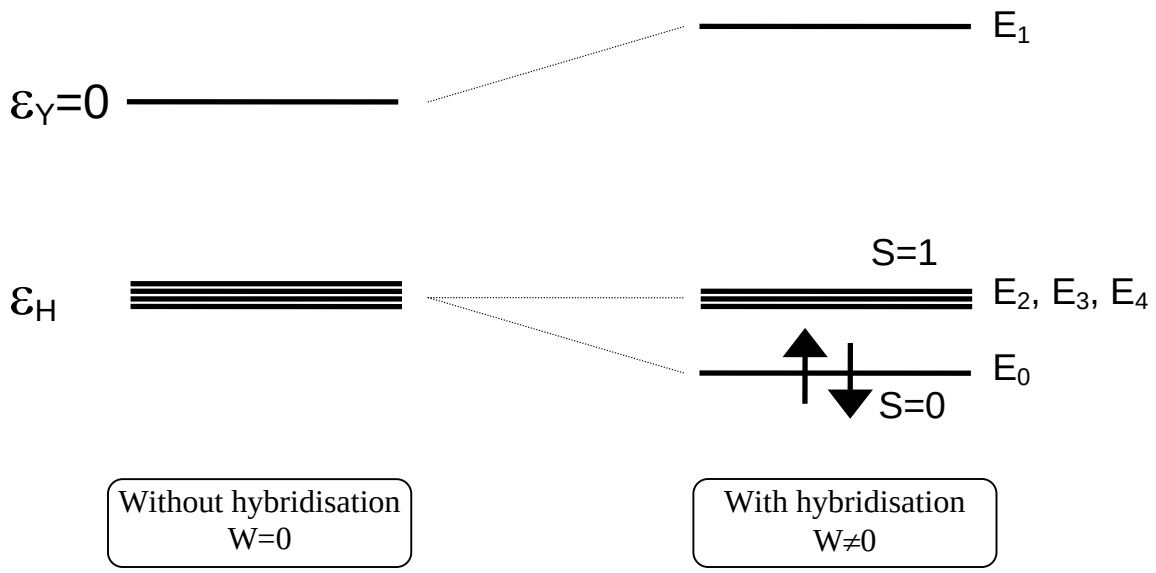

Fig. VI.23: Influence of hybridisation on the total energy of a diatomic molecule where double occupation of the hydrogen orbital is forbidden.

For situations where both U_H and W differ from zero we need to solve the cubic equation VI.87. We give in Fig. VI.24 the energies of the three levels E_0, E_1, and E_2 calculated for parameters which might be relevant to the problem of hydrogen in yttrium, i.e. ε_H=-4 eV, W=2 eV and U_H between 0 and 6 eV (because of screening we do not need to consider higher values for the Coulomb repulsion term on the hydrogen). For comparison we have also indicated the levels for the case where both W and U_H are zero.

The main difference is that the two lowest states interact with each other due to the hybridisation term. When Coulomb repulsion is zero i.e. when U_H=0, the ground state is evidently $2\varepsilon_H$=-8 eV minus an energy gain due to hybridisation. When U_H increases and double occupation of the hydrogen orbital becomes increasingly more difficult the ground state resembles more and more a state where one electron is mainly localised on H and the other on Y. One should, however, not forget that even in the case of infinite U_H hybridisation allows for a certain amount of delocalisation of the electrons and therefore lowers their total energy. Consequently, as discussed above (see Eq.VI.91) the total energy remains **below** $\varepsilon_{H+}\varepsilon_Y$=-4 eV. In Fig. VI.24 only three levels are indicated. The other three levels are unaffected by W or U_H and have an energy equal to $\varepsilon_{H+}\varepsilon_Y$=-4 eV. For hydrogen in yttrium metal these states would correspond to those d-band states which are not affected by hydrogen. Independently of the value of U_H, Fig. VI.24 demonstrates that there is a low-lying state below the d-band of the host metal.

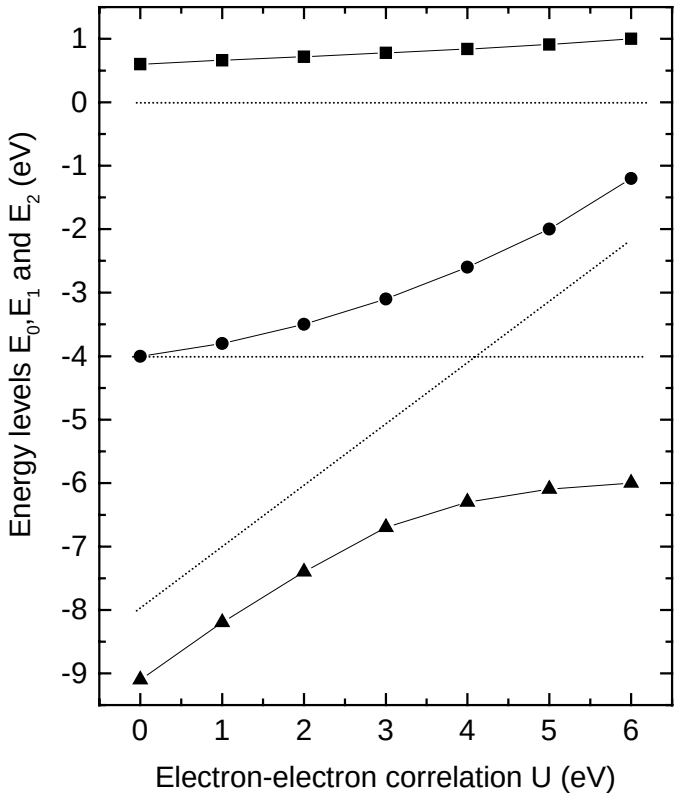

Fig. VI.24: Energy levels for a diatomic molecule with two electrons. The hybridisation term is chosen as W=2 eV and U varies from zero to 6 eV. The dotted lines correspond to the situation without hybridisation (W=0).

VI.6.4 THE BREATHING ORBITAL MODEL.

Recently Eder et al introduced the so-called **breathing orbital model** for the electronic structure of YH_3 . The idea of this model is strongly inspired by the results of Chandrasekhar for the H^- ion. From Eq.VI.61 we know that electrons in the H^- ion occupy two orbits with vastly different radii, r_{in}=0.0492 nm and r_{out}=0.1108 nm. As a first approximation one can therefore assume for the overlap that

$$\begin{aligned}
&\left\langle \left[d_1 s_2 \pm d_2 s_1 \right] \middle| V_A(i) \middle| \left[d_1 s_2 \pm d_2 s_1 \right] \right\rangle = 0 \text{ for A = H, Y} \\
&\left\langle \left[d_1 s_2 \pm d_2 s_1 \right] \middle| V_A(i) \middle| d_1 d_2 \right\rangle = 0 \\
&\left\langle \left[d_1 s_2 + d_2 s_1 \right] \middle| V_A(i) \middle| s_1 s_2 \right\rangle \equiv V_1 \neq 0 \text{ for A = H} \\
&\left\langle s_1 \middle| d_1 \right\rangle = \left\langle s_2 \middle| d_2 \right\rangle = 0 \\
&\left\langle d_1 d_2 \middle| V_{12} \middle| d_1 d_2 \right\rangle \cong 0 \\
&\left\langle s_1 s_2 \middle| V_{12} \middle| s_1 s_2 \right\rangle = U_H
\end{aligned} \qquad \text{(VI.93}$$

where we have used Eder et al's notation for the overlap integral between the singlet state and the s-orbitals of the H^- ion. The physical picture behind these approximations is simply that the overlap integrals involving the very large H^- ion are much larger than those involving the s-orbital of the neutral hydrogen atom. The breathing orbital model (in its simplest form) is thus a special case of our treatment of the diatomic molecule. Their results can immediately be derived from

$$\begin{vmatrix}
(\varepsilon_Y + \varepsilon_H) - E & 0 & 0 & 0 & 0 & \sqrt{2}V_1 \\
0 & (\varepsilon_Y + \varepsilon_H) - E & 0 & 0 & 0 & 0 \\
0 & 0 & (\varepsilon_Y + \varepsilon_H) - E & 0 & 0 & 0 \\
0 & 0 & 0 & (\varepsilon_Y + \varepsilon_H) - E & 0 & 0 \\
0 & 0 & 0 & 0 & (2\varepsilon_Y - E) & 0 \\
\sqrt{2}V_1 & 0 & 0 & 0 & 0 & (2\varepsilon_H + U_H - E)
\end{vmatrix} = 0 \qquad \text{(VI.94}$$

which leads to the following energy levels (if we set ε_Y=0)

$$\begin{aligned}
E_0 &= \varepsilon_H + \frac{\varepsilon_H + U_H - \sqrt{(\varepsilon_H + U_H)^2 + 8V_1^2}}{2} \\
E_1 &= \varepsilon_H + \frac{\varepsilon_H + U_H + \sqrt{(\varepsilon_H + U_H)^2 + 8V_1^2}}{2}
\end{aligned} \qquad \text{(VI.95}$$

$$E = 0 \qquad \text{(VI.96}$$

$$E = \varepsilon_H \qquad \text{(VI.97}$$

the last one being threefold degenerate. In Eder et al's notation ε_H=-Δ, so that

$$E_0 = -\Delta + \frac{U_H - \Delta}{2} - \sqrt{\left(\frac{U_H - \Delta}{2}\right)^2 + 2V_1^2}$$

$$E_1 = -\Delta + \frac{U_H - \Delta}{2} + \sqrt{\left(\frac{U_H - \Delta}{2}\right)^2 + 2V_1^2} \qquad \text{(VI.98}$$

$$E = -\Delta$$

As U_H and Δ are usually of the same order of magnitude they conclude that the overlap involving the H^- ion orbitals is the essential parameter in the theory. The fact that an overlap depends on the occupation of the orbital under consideration (in our case the H^- ion orbital) was shown to lead to essential corrections to the electronic structure of YH_3.

VI.7 NEW BAND STRUCTURE CALCULATIONS

Several theorists[11, 27, 28] have recently calculated the electronic structures of YH_3 using band structure codes that incorporate electron correlation effects. These codes, based on the so-called GW-approximation or on the all-electron full-potential method enhanced by screened-exchange local-density-approximation are able to reproduce the semiconducting state of YH_3 and its optical properties. Interesting is also that the results seem to be remarkably insensitive to the assumed crystal structure in contrast to what was claimed by Kelly et al in their Peierls transition model (see Fig. VI.25). This seems to show that after six years of work theorists have now band structure codes that are able to make quantitative predictions for YH_3 and probably for all the REH_3.

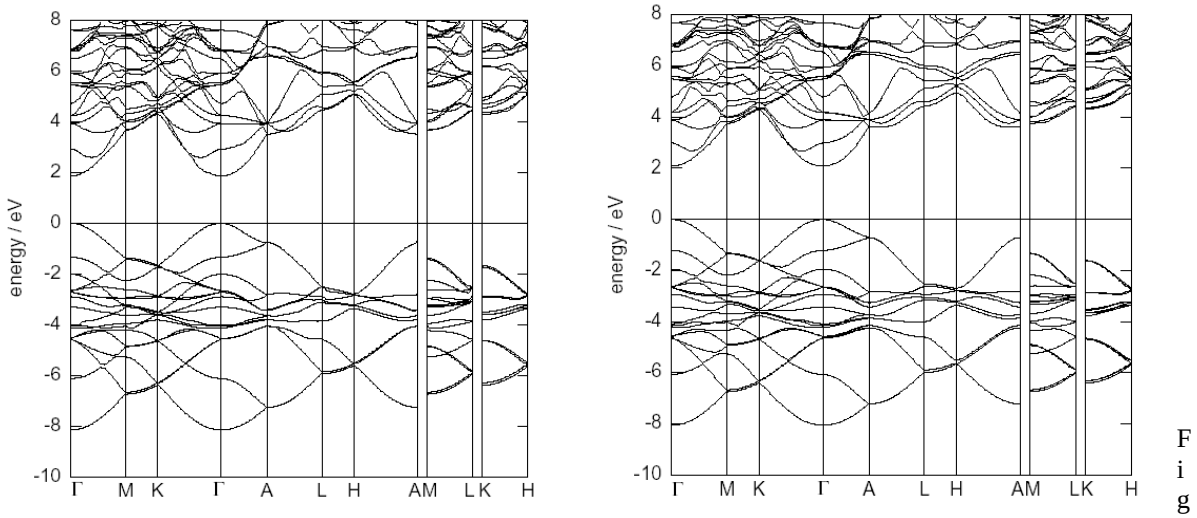

Fig. VI.25. Band structures for YH_3 obtained by Herzig et al using the all-electron full-potential method enhanced by screened-exchange local-density-approximation[28]. In the left panel the structure of YH_3 is assumed to be $P6_3cm$, while in the right panel it is $P6_3$. Interestingly the structure has little influence on the magnitude of the energy gap.

In summary I have tried in this section to give an idea of the basic concepts which are essential for the understanding of the electronic structure of YH_x, LaH_x and RE metal-hydride systems. There are, however, still important questions about the nature of the metal-insulator transition that cannot be tackled with band structure approaches since doping introduces necessarily disorder. The fact that optical switching is seen not only in Yttrium and lanthanum hydrides, but also in all the rare-earths hydrides and in hydrides of alloys containing rare-earths and magnesium seem to indicate that the optical switching is a robust phenomenon which depends mainly on the immediate environment of the hydrogen. This seems to favour an approach based on strong electron correlation effects.

VI.8 REFERENCES

[1] G.G. Libowitz and J.G. Pack, J. Chem. Phys. 50 (1969) 3557
[2] G.G. Libowitz, Ber. Bunsen Ges. Phys. Chem. 76 (1972) 837
[3] J. Shinar, B. Dehner, R.G. Barnes and B.J. Beaudry, Phys. Rev. Lett. 64 (1990) 563
[4] A.F.Th. Hoekstra, A.S. Roy, T.F. Rosenbaum, R. Griessen, R. Wijngaarden and N.J. Koeman, Phys. Rev. Lett. 86 (2001) 5349-5352
[5] R. Griessen, Europhysics News (2001) Vol. 32 No. 2
[6] R. Griessen, I.A.M.E. Giebels and B. Dam, to be published by Wiley (edited by A. Züttel)
[7] J.N. Huiberts, R. Griessen, J.H. Rector, R.J. Wijngaarden, J.P. Dekker, D.G. de Groot, and N.J. Koeman, Nature (London) 380, 231 (1996)
[8] P. Vajda: "Hydrogen in Rare-Earth Metals including RH2+x phases" in Handbook on the Physics and Chemistry of Rare Earths 20, 207 (Elsevier Science 1995) and references therein
[9] F.J.A. den Broeder, S.J. van der Molen, M. Kremers, J.N. Huiberts, D.G. Nagengast, A.T.M. van Gogh, W.H. Huisman, J.P. Dekker, N.J. Koeman, B. Dam, J.H. Rector, S. Plota, M. Haaksma, R.M.N. Hanzen, R.M. Jungblut, P.A. Duine, and R. Griessen, Nature (London) 394, 656 (1998)
[10] A.T.M. van Gogh, D.G. Nagengast, E.S. Kooij, N.J. Koeman, and R. Griessen Phys. Rev. Lett. 85, 2156 (2000)
[11] P. van Gelderen, P. A. Bobbert, P. J. Kelly, G. Brocks, Phys. Rev. Lett. 85, 2989 (2000) and references therein.
[12] R. Eder, H.F. Pen, and G.A. Sawatzky, Phys. Rev. B 56, 10115 (1997);
[13] K.K. Ng, F.C. Zhang, V.I. Anisimov, and T.M. Rice, Phys. Rev. Lett. 78, 1311 (1997) and Phys. Rev. B. 59, 5398 (1999)
[14] S. J. van der Molen, M. S. Welling and R. Griessen, Phys. Rev. Lett. 85, 3882 (2000)
[15] R. Griessen and P. van der Sluis, Schaltbare Spiegel, Physik in unserer Zeit (2), (2001) and references therein.
[16] P. van der Sluis, M. Ouwerkerk, and P.A. Duine, App l. Phys. Lett. 70, 3356 (1997)
[17] T.J. Richardson, J.L. Slack, R.D. Armitage, R. Kostecki, B. Farangis, and M.D. Rubin, Appl. Phys. Lett. 78 (2001) 3047
[18] J. W. J. Kerssemakers, S. J. van der Molen, N. J. Koeman, R. Günther and R. Griessen, Nature 396, 489 (2000)
[19] A.C. Switendick, Internat. J. Quantum Chem. 5 (1971) 459
[20] J. P. Dekker, J. van Ek, A. Lodder, J. N. Huiberts, J. Phys.: Condens. Matter 5 (1993) 4805.
[21] Y. Wang, M. Y. Chou, Phys. Rev. B 51 (1995) 7500.
[22] P. J. Kelly, J. P. Dekker, R. Stumpf, Phys. Rev. Lett. 78 (1997) 1315.
[23] Bethe, H., Zs. f. Phys. 57 (1929) 815 and Bethe, H., Proc. Roy. Soc. A 150 (1935) 552
[24] Hylleraas, E. A., Zs. f. Physik. 60 (1930) 624
[25] Chandrasekhar, S., Astrophys. J. 100 (1944) 176
[26] M.B.J. Meinders, H. Eskes and G.A. Sawatzky, Phys. Rev. B48 (1993) 3916
[27] T. Miyake, F. Aryasetiawan, H. Kino, K. Terakura, Phys. Rev. B 61 (2000) 16491.
[28] P. Herzig, private communication (2002)